Geochemistry, Geophysics, Geosystems

RESEARCH ARTICLE
10.1029/2019GC008795

Silica-Rich Vein Formation in an Evolving Stress Field, Atlantis Bank Oceanic Core Complex

Qiang Ma[1], Henry J. B. Dick[1,2], Benjamin Urann[2], and Huaiyang Zhou[1]

[1]State Key Laboratory of Marine Geology, Tongji University, Shanghai, China, [2]Department of Geology and Geophysics, Woods Hole Oceanographic Institution, Woods Hole, MA, USA

Key Points:
- Felsic veins in the Atlantis Bank gabbro batholith represent igneous and anatectic origins at high and low temperatures, respectively
- They have different formation temperature, fO_2, and Fl-Cl ratios, reflecting the presence igneous and seawater-derived volatiles
- They formed during compression and extension, respectively, consistent with asymmetric intrusion of the gabbro during detachment faulting

Supporting Information:
- Supporting Information S1
- Table S1
- Table S2
- Table S3
- Table S4
- Table S5
- Table S6
- Table S7

Correspondence to:
H. J. B. Dick and H. Zhou,
hdick@whoi.edu; zhouhy@tongji.edu.cn

Citation:
Q. Ma, H. J. B. Dick, B. Urann, & H. Zhou (2020). Silica-rich vein formation in an evolving stress field, Atlantis Bank Oceanic core complex. Geochemistry, Geophysics, Geosystems, 21, e2019GC008795. https://doi.org/10.1029/2019GC008795

Received 6 NOV 2019
Accepted 8 JUN 2020
Accepted article online 14 JUN 2020

Abstract Drilling 809-m Hole U1473A in the gabbro batholith at the Atlantis Bank Oceanic Core Complex (OCC) found two felsic vein generations: late magmatic fractionates, rich in deuteric water, hosted by oxide gabbros, and anatectic veins associated with dike intrusion and introduction of seawater-derived volatiles. Microtextures show a change from compressional to tensional stress during vein formation. Temperatures and oxidation state were obtained from amphibole-plagioclase and oxide pairs in the adjacent gabbros. Type I veins generally have reverse shear-sense, with restricted ΔFMQ, high Mt/Ilm ratios, and low-amphibole Cl/F indicating deuteric fluids. They formed during percolation and fractionation of Fe-Ti-rich melts into the primary olivine gabbro. Type II veins are usually hosted by olivine gabbro, occur at dike contacts and the margins of normal-sense shear zones. They are undeformed or weakly deformed, with highly variable ΔFMQ, low Mt/Ilm ratios, and high-amphibole Cl/F, indicating seawater-derived fluids. The detachment fault on which the gabbro massif was emplaced rooted near the base of the dike-gabbro transition beneath the rift valley. The ingress of seawater volatiles began at >800°C and penetrated at least ~590 m into the lower crust during extensional faulting in the rift valley and adjacent rift mountains. The sequence of the felsic vein formation likely reflects asymmetric diapiric flow, with a reversal of the stress regime, and a transition from juvenile to seawater-derived volatiles. This, in turn, is consistent with fault capture leading to the large asymmetries in spreading rates during OCC formations and heat flow beneath the rift mountains.

1. Introduction

Felsic veins including anorthosite, diorite, quartz diorites, tonalities, and trondhjemites, also termed oceanic plagiogranites, are ubiquitous in abyssal gabbros in oceanic core complexes (OCCs) at slow-spreading and ultraslow spreading ridges, and ophiolites (Blackman et al., 2006; Coleman & Peterman, 1975; Robinson et al., 1989). They are products of late-stage magmatic evolution in the lower crust, generated by differentiation of mid-ocean ridge basalt (MORB) (Berndt et al., 2005; Chen et al., 2019; Coleman & Peterman, 1975; Feig et al., 2006; Grimes et al., 2011; Nguyen et al., 2018; Niu et al., 2002), partial melting of hydrated gabbros (Dick, Meyer, et al., 1991; Flagler & Spray, 1991; Koepke et al., 2004, 2005, 2007), or liquid immiscibility (Dixon & Rutherford, 1979; Natland et al., 1991). As such, they can provide critical information on the evolution of the lower ocean crust, constraining the final stages of its accretion and emplacement, reflecting the relationship between the late-stage magmatic and internal structural evolution of the lower ocean crust.

The origins of felsic veins can be constrained by the relative Cl and F contents in amphibole (Coogan et al., 2001; Kendrick, 2019), and their oxidation states as inferred from ilmenite-titanomagnetite pairs (Andersen et al., 1993) where these minerals are common major or accessory phases in or next to felsic veins. Magmatic water behaves incompatibly during fractional crystallization of MORB, which affects the oxygen fugacity (fO_2) and controls oxide precipitation (Berndt et al., 2005; Feig et al., 2006; Koepke et al., 2018; Toplis & Carroll, 1995; Zimmer et al., 2010). Thus, a difference in fO_2 at multiple stages of crystallization may produce felsic melts either by fractionation or liquid immiscibility in the residual melt (Berndt et al., 2005; Dixon & Rutherford, 1979; Feig et al., 2006; Koepke et al., 2018; Natland et al., 1991). Felsic melts produced by hydrous anatexis of lower oceanic crust may occur due to either concentration of late magmatic (deuteric) fluids or due to infiltration of Cl-rich seawater-derived volatiles. These origins can then be distinguished by higher and lower F-Cl ratios, respectively.

Table 1
Summarized Characteristics Comparing Different Types of Felsic Veins in This Study

Type	Origin	Deformation	Host gabbro dominated	Mag-ilm ratio	Oxidation state	Oxide thermometry	Plag-amph thermometry	Cl/F ratio	Plagioclase in host gabbro
I	Magmatic fractionates	Reverse-sense	Oxide gabbro	>0.5	0–2.8	>600°C	800–900°C	<0.1	Albite-rich rims
II	Hydrous partial melting	Normal-sense	Olivine gabbro	<0.5	0–5.4	<580°C	650–800°C	>0.1	Anomalous anorthite-rich
Trondhjemite	Magmatic fractionates	Undeformed	Olivine gabbro	>0.5	2.02	~645°C	~708°C	<0.1	
Dike contact	Hydrous partial melting	Undeformed	Olivine gabbro	<0.5	−1.4–0.13	577–608°C	875–925°C	>0.1	

Previous studies of amphibole halogen contents and fO_2 associated with natural silica-rich melt formation are scarce (Kendrick, 2019; Koepke et al., 2005). In part, this is because felsic veins are generally more strongly altered than their host rocks (MacLeod, et al., 2017a), where this can overprint the original fluid and the fO_2 signals. At Atlantis Bank, interactions between felsic melts and the host gabbro are common, and formation of felsic rocks are strongly controlled by temperature conditions of the host gabbros (Nguyen et al., 2018). In addition, microstructures, such as the character of deformation, sense of shear, and crosscutting relationships can provide key information on the timing and conditions of vein formation, although this information may only be well recorded in the host gabbros (Koepke et al., 2004, 2005). Thus, we focus on the microstructures, oxidation states, amphibole halogen concentrations, and temperatures in the adjacent wall rocks, showing that these reflect the conditions of vein formation. Here we present a study of felsic veins in the Atlantis Bank OCC, using microtextures, plagioclase, and amphibole compositions, including F and Cl, equilibrium temperatures using the amphibole-plagioclase geothermometer of Holland and Blundy (1994), and magnetite/ilmenite ratios and oxidation states determined from ilmenite-titanomagnetite pairs. Details are listed in Table 1. The petrogenesis of the vein sets are consistent with an evolving stress field during gabbroic intrusion and diapirism, first, in a still partially molten gabbro, and later by postsolidification hydrous partial melting following the ingress of seawater-derived fluids, which then is intimately related to the nature of detachment faulting and asymmetric spreading at the ridge axis.

2. Geological Background

Atlantis Bank is located 95 km south of Southwest Indian Ridge flanking the eastern wall of the Atlantis II FZ. It formed beginning at ~13 Ma (Dick, Schouten, et al., 1991; John et al., 2004; Schwartz et al., 2005; Rioux et al., 2016) highly asymmetric spreading of 14.1 mm/yr to the south and 3.5 mm/yr to the north (Baines et al., 2008) (Figure 1a). It is a 660-km^2 gabbro batholith, considerably thicker than the 1.5 km drilled to date at its midpoint, intruded into massive mantle peridotite for ~30 km along the wall of the Atlantis II Transform (Dick, Kvassnes, et al., 2019). It was uplifted above sea level by a combination of bending stresses at the ridge-transform intersection, and flexural uplift associated with two transform-parallel normal faults on its eastern flank (Figure 1b). The latter formed consequent to a spreading direction change and dilation across the transform (Baines et al., 2003; Dick, Schouten, et al., 1991).

OCCs form by detachment faulting exposing lower crust and mantle from beneath a rift valley floor (Cann et al., 1997; Dick et al., 1981; Dick, Schouten, et al., 1991). Detachment faults generally initiate as high-angle normal faults with dips up to ~70° and rotate progressively to lower angles as they grow. With prolonged displacement, the footwall rolls over to create a core-complex dome on the seafloor (e.g., deMartin et al., 2007; Morris et al., 2009). Long-lived detachment faults can represent millions of years of displacement, as for Atlantis Bank (~2.7 Myr), with footwall dips rotating to 0°, and even to negative angles far from the ridge axis (MacLeod et al., 2009). While plate separation is accommodated at fast-spreading ridges (> ~50 mm/yr) largely by magmatic accretion, at slow and ultraslow spreading ridges it is accommodated by both magmatic accretion and tectonic extension (e.g., Mutter & Karson, 1992). The latter is accommodated in turn by brittle deformation above the brittle-ductile transition, and crystal-plastic deformation and crystal mush flow below it.

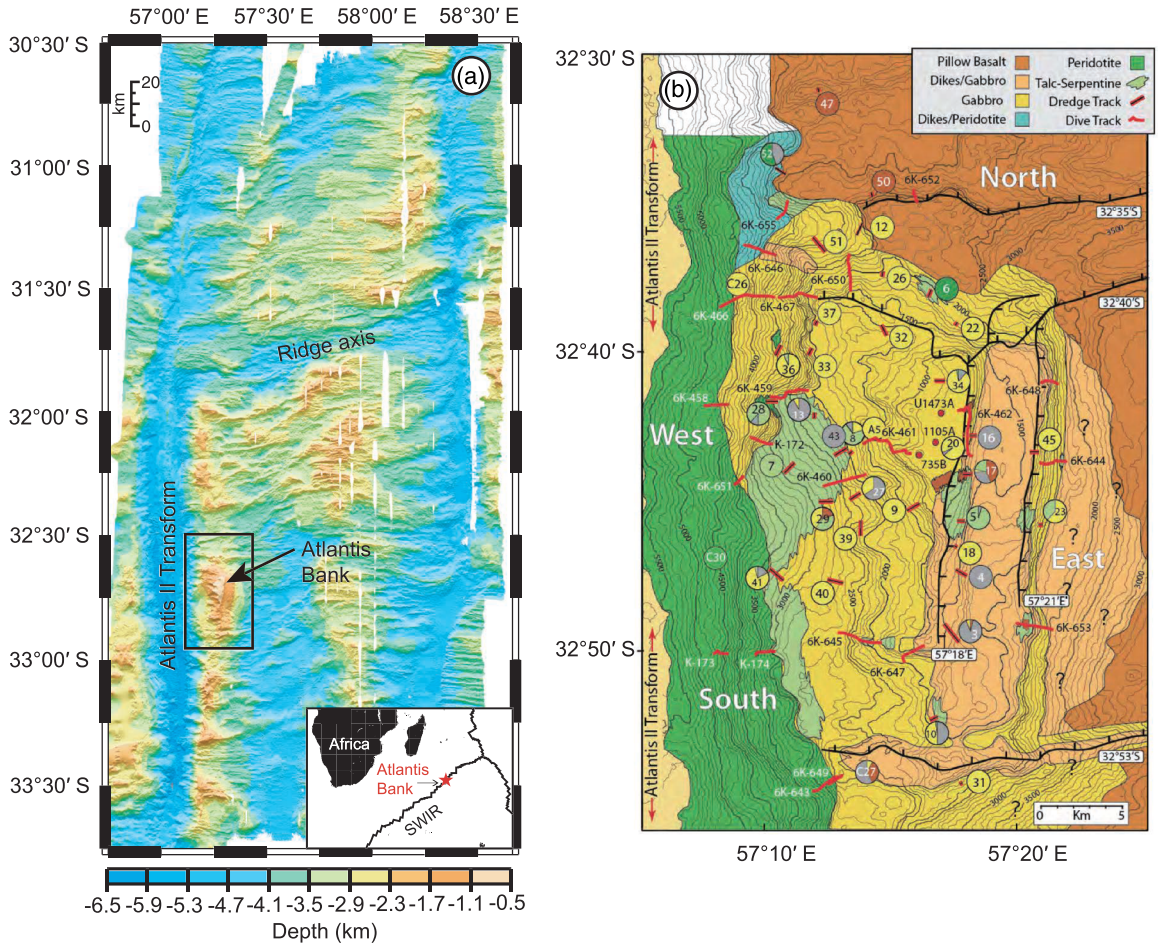

Figure 1. (a) Bathymetry map, contoured at 500-m interval, showing the position of Atlantis Bank relative to Atlantis II transform and ridge axis. Regional map at lower right corner showing the location of Atlantis Bank on SWIR. After Hosford et al. (2003). The black rectangle marks the survey area in (b) geological map of Atlantis Bank. The locations of Hole 735B, Hole 1105A, and Hole U1473A are shown by red dots, after Dick, Kvassnes, et al. (2019).

Microtextures at Atlantis Bank (Dick et al., 2000; Dick, Schouten, et al., 1991; Miranda & John, 2010; Natland & Dick, 2001) and at the Mid-Atlantic Ridge at 23°N (Agar & Lloyd, 1997) show that crystal-plastic deformation extends from the solid-state into the hypersolidus region where melt fractions are low. This has led to the formation of shear zones, which provided conduits for late-stage melt migration resulting in the transformation of olivine gabbro to oxide gabbro (Dick, Kvassnes, et al., 2019; Dick, Meyer, et al., 1991; Lissenberg & MacLeod, 2016). Later, active shear zones also localized hydrothermal fluids, leading to the formation of sheared amphibolites. Notably, where the detachment fault is uneroded over Atlantis Bank, the footwall consists of a 1-m layer of talc-serpentine schist, underlain by an oxide-gabbro mylonite layer. The latter indicating that the fault rooted into partially molten gabbro (Dick, Kvassnes, et al., 2019), with the fault later lubricated by intrusion of talc-serpentine schist along the fault plane.

Somewhat irregularly spaced, locally pervasive, high-temperature crystal-plastic deformation is found throughout the drill cores (Dick et al., 1999; Dick, MacLeod, et al., 2019; MacLeod, Dick, Blum, Abe, Blackman, Bowles, Cheadle, Cho, Ciazela, Deans, Edgcomb, Ferrando, France, Ghosh, Ildefonse, Kendrick, Koepke, Leong, Liu, et al., 2017a). In Hole 735B, crystal plastic deformation broadly increases from the bottom of the hole, where it is intermittent and weak below 1,000 mbsf, to its highest intensity in the upper 150 m. Hole U1473A is consistent with an upward increase in crystal-plastic deformation in the gabbro massif, as it is broadly similar to the upper 800 m of Hole 735B with crystal-plastic

deformation dropping off below 700 m, while lacking the intense zone of deformation found in the upper 150 m of Hole 735B, likely due to erosion.

Vanko and Stakes (1991) found that for a depth of 4,000 m, corresponding to the modern Southwest Indian Ridge rift valley, the lithostatic pressure for a sample from core 735B-R70 indicated from fluid inclusions would be 1.7 to 2.0 km below the seafloor. If the rift valley were significantly shallower, then the estimated overburden would be greater. This sample was taken at ~350 mbsf (meters below seafloor), thus there would have been 1.35 to 1.65 km of overburden that was removed by detachment faulting. With abundant cataclastic diabase recovered from the seafloor around Atlantis Bank, there is abundant evidence that this included a massive sheeted dike complex (Dick, Kvassnes, et al., 2019). While there are inliers of the dike-gabbro transition in the detachment footwall, however, only 5 m of diabase out of 2,200 m of core were recovered by drilling. This indicates that there was no melt lens, but a fairly sharp dike-gabbro transition of a few hundred meters where crosscutting dikes are intercalated with gabbro screens (Dick, Kvassnes, et al., 2019) (Figure 1b). This shows that the detachment fault passed through close to the base of the dike-gabbro transition and into the underlying partially molten gabbro.

The gabbro massif formed by a dynamic process of intermittent intrusion during ongoing extension driven by plate separation. Intercumulus liquid was redistributed due to compaction-driven permeable flow both vertically and laterally prior to complete solidification, with localized flow into shear zones subsequently enriching them in Fe-Ti oxides (Dick et al., 2000; Dick, Kvassnes, et al., 2019; Dick, Meyer, et al., 1991). Three Ocean Drilling Program (ODP) and International Ocean Discovery Program (IODP) drill holes (1,508-m Hole 735B, 158-m Hole1105A, and 809-m Hole U1473A) were drilled near the center of the gabbro massif over a ~2.2-km interval near a single lithospheric flow line (MacLeod, Dick, Blum, Abe, Blackman, Bowles, Cheadle, Cho, Ciazela, Deans, Edgcomb, Ferrando, France, Ghosh, Ildefonse, Kendrick, Koepke, Leong, Liu, et al., 2017b; Figure 1b). The felsic veins and patches discussed here occur ubiquitously, but comprise only ~0.5% and 1.5% of the Hole 735B and U1473A lithologies (Dick et al., 2000; MacLeod, Dick, Blum, Abe, Blackman, Bowles, Cheadle, Cho, Ciazela, Deans, Edgcomb, Ferrando, France, Ghosh, Ildefonse, Kendrick, Koepke, Leong, Liu, et al., 2017).

3. Samples and Methods

3.1. Samples

3.1.1. General Descriptions and Representative Structures in Hole U1473A

To investigate the relationships between deformation processes and origins of felsic veins, this study mainly focuses on foliated gabbros hosting felsic veins with different shear sense. As listed in Table S1 in the supporting information, five normal-sense sheared and five reverse-sense sheared felsic veins form Hole U1473A were studied. The shear sense for felsic veins show a transition from normal to reverse at depth of ~ 640 mbsf in Hole U1473A (Figure 2c), while similar transition in foliated gabbros occurs at ~50 mbsf (Figure 2b). Then, the dominant shear sense for felsic veins and gabbros are different over the region of ~180–440 mbsf. It reflects tectonic processes associated with their formation that likely have chronological relationships. This is confirmed by observations of normal-sense sheared felsic veins cross-cutting reverse-sense sheared gabbros (Table S3 and section 3.2.3). For comparison, a reverse-sense sheared felsic vein from this structurally overlapping region (25R-2 42–42.5 cm), and its textural and geochemical characteristics differ from those of normal-sense sheared veins (Tables S1 and S6). The rest of the reverse-sense felsic veins in our study are from depth of below ~640 mbsf, where reverse-shear sense is dominant in both gabbros and felsic veins (Figures 2b and 2c). Therefore, our sample set is suitable to represent the deformation processes related to felsic vein formation. Four undeformed felsic veins are also studied, including two samples in contact with dikes, and two trondhjemites (Table S1). Moreover, four unveined reverse-sense foliated oxide gabbros and five undeformed oxide gabbronorites from below ~90 mbsf were also included, corresponding to a reverse-shear sense-dominated region in gabbro (Figure 2b). Most of the foliated gabbros have intensity rank ranging from Grade 3 (protomylonite) to Grade 5 (ultramylonite) on the IODP Expedition 360 textural deformation scale (MacLeod, et al., 2017b). The shear sense, true dip, and crystal-plastic fabrics (CPFs) intensities for the gabbros and felsic veins were mostly taken from the shipboard macroscopic descriptions, together with additional data from our personal sample sets. Dick, Meyer, et al. (1991) found that gabbros containing >1% oxides were generally distinct geochemically from gabbro and olivine gabbro with <1% oxides, being

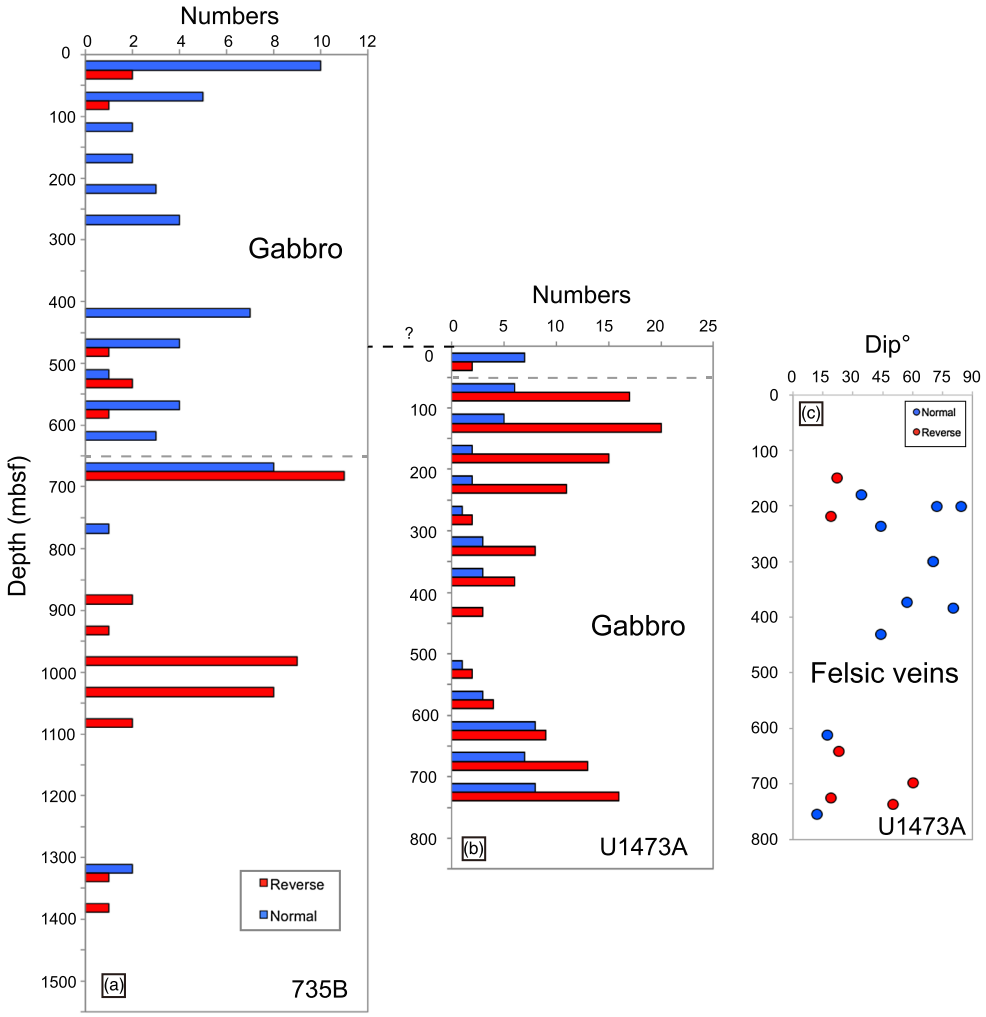

Figure 2. Downhole distribution of shear sense indicators for crystal plastic fabrics in gabbros and felsic veins. The numbers of different indicators are plotted as histograms with a 50-m spacing. The gray dash lines show the approximate transition depth from normal to reverse sense, while the black dash line with a question mark indicates a possible depth correlation between Holes 735B and U1473A based on a chemical discontinuity in the cores. (a) Hole 735B gabbros, data from Cannat et al. (1991) and Dick et al. (1999); (b) Hole U1473A gabbros, data from Exp360 shipboard macroscopic descriptions with additional data from our thin section observations; (c) down hole shear sense and dip of felsic veins in Hole U1473A.

generally iron-titanium rich, and highly evolved. Accordingly, we include here as "oxide gabbro" all gabbros with >1% oxide and olivine gabbro as gabbros with variable olivine contents with <1% oxides.

3.2. Methods

3.2.1. Electron Microprobe Analysis

Oxide, plagioclase, and hornblende major element compositions including F and Cl were determined by five wavelength-dispersive spectrometers on a JEOL JXA-8200 Superprobe at MIT, using 15 kV accelerating voltage and 10 nA beam current. Beam size was 1 um for oxides, and 3 μm for hornblende and plagioclase. The counting times were 40 s for each element except Na, which was 10 s. For plagioclase, the standards used were Synthetic Anorthite (Si, Al, Ca), Amelia Albite (Na), and Orthoclase glass (K). For oxides, hematite (Fe), rutile (Ti), uvarovite (Cr), rhodonite (Mn), and NiS (Ni) were used. The standard deviations of major elements were typically between 0.25–1% relative to the counts. F and Cl were counted for 10 and 40 s, respectively. Standards for hornblende were synthetic diopside-jadeite (Si, Al, Mg, Ca, Na), synthetic

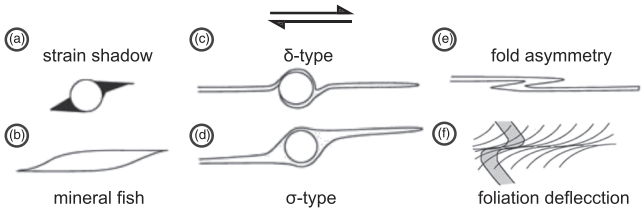

Figure 3. The schematic geometry of shear sense indicators under a dextral shear sense, after Passchier and Trouw (2005).

orthopyroxene (Fe), fluorphlogopite (F), and sodalite (Cl). The detection limits for F and Cl are ~510 and 52 ppm, respectively, and their standard deviations were typically between 5% and 10%. Up to four spots on the oxides and up to six spots (from core to rim) on hornblende and plagioclase were analyzed. Where mineral grain size was small, one spot on each mineral phase was analyzed on several grains and averaged.

3.2.2. Thermometry

Equilibrium temperatures were determined by amphibole-plagioclase thermometry (Holland & Blundy, 1994), while those of ilmenite-titanomagnetite pairs together with their oxidation states were calibrated using QUILF program (Andersen et al., 1993). The amphibole-plagioclase calculated temperatures are insensitive to pressures (Miranda & John, 2010). Similarly, pressure has negligible effect on calculated temperatures and fO_2 (Andersen et al., 1993), where 1 kbar difference in pressure will result in ~0.1 variation of **Δ**FMQ. Thus, we use the results calibrated at 1 kbar for consistency in this study.

3.2.3. Determination of Shear Sense

Various indicators are important tools to determine the shear sense. The common types of shear-sense indicators under dextral shear sense are shown in Figure 3. The certainty of shear-sense determination is based on the shipboard principle (MacLeod, et al., 2017b). Shear-sense data obtained by Exp 360 shipboard macroscopic descriptions and those determined by our thin section observations (Table S2) are both included. Where differences of shear sense exist between macroscopic descriptions and thin section observations in the same fabric interval, shear-sense data measured on the thin sections were used.

We attempt to investigate the relative formation timing of sheared samples with different senses using their cross-cutting relationships. Clear cross-cutting relationships with well-determined shear sense are found in four shipboard thin sections (Table S3). Normal shear-sense zones cross-cutting porphyroclastic gabbros with a reverse shear sense are observed in three of them, whereas one reverse-sense sheared gabbro is transposed by a narrow shear zone having the same shear sense. However, paleomagnetic inclination data from Hole U1473A reveal that a tectonic rotation up to 12° below the Curie temperature has occurred (Morris et al., 2016). With this amount of rotation, the shear-sense indicator might itself be rotated sufficiently to give an opposing shear sense (<12° or >78°). Therefore, shear senses of these foliated samples are reexamined by applying both clockwise and anticlockwise rotation of 12°. Subsequent to applying an anticlockwise rotation of 12°, relative cross-cutting relationships remain unchanged. Interestingly, all of the four shipboard thin sections are reverse shear-sense porphroclastic gabbros that are transposed by normal shear-sense zones, following a clockwise rotation of 12°. For instance, in Sample 23R-3 65–73 cm, a normal shear-sense felsic vein (along the right margin of a normal-sense shear zone) has a dip of 72°, and cross-cuts a reverse shear-sense olivine gabbro with a dip of 21° (Figure 4a). The shear sense remains the same by applying either clockwise or anticlockwise rotation of 12°. Based on these cross-cutting relationships, we suggest that deformation processes forming CPF's with a reverse shear sense likely occur prior to that related to the formation of normal-sense sheared CPFs.

3.2.4. Validity of Methods

To test the degree with which the conditions of vein formation can be estimated from wall rocks, we analyzed a profile from a veined oxide gabbro with a reverse shear sense in Core 82R-3, 93–114 cm down core into the adjacent gabbro. Figure 5a shows that there is a gradient in **Δ**FMQ and oxide-pair equilibrium temperatures where **Δ**FMQ increases up core toward the felsic vein, whereas the equilibrium temperature decreases. Moreover, a gradient in amphibole-plagioclase equilibrium temperatures was also obtained, where temperatures decrease up core toward the veined oxide gabbro. Nevertheless, amphiboles show a slight decrease up core toward veined oxide gabbro in their F contents, but no significant variations in their Cl concentrations, which are below the detection limit.

At the same time, amphibole halogen contents measured in a second normal-sense sheared oxide gabbro (Core 85R-3 37–49 cm) shown in Figure 5d are similar to those of felsic veins, whereas the equilibrium temperature by amphibole-plagioclase thermometer is moderately higher (Figure 5e). In a normal-sense sheared felsic vein at shallower depth (20R-2 68–74 cm), amphibole Cl concentrations are 120–245 ppm, which is slightly higher than that measured for amphibole in host olivine gabbro (75–140 ppm). Their F contents

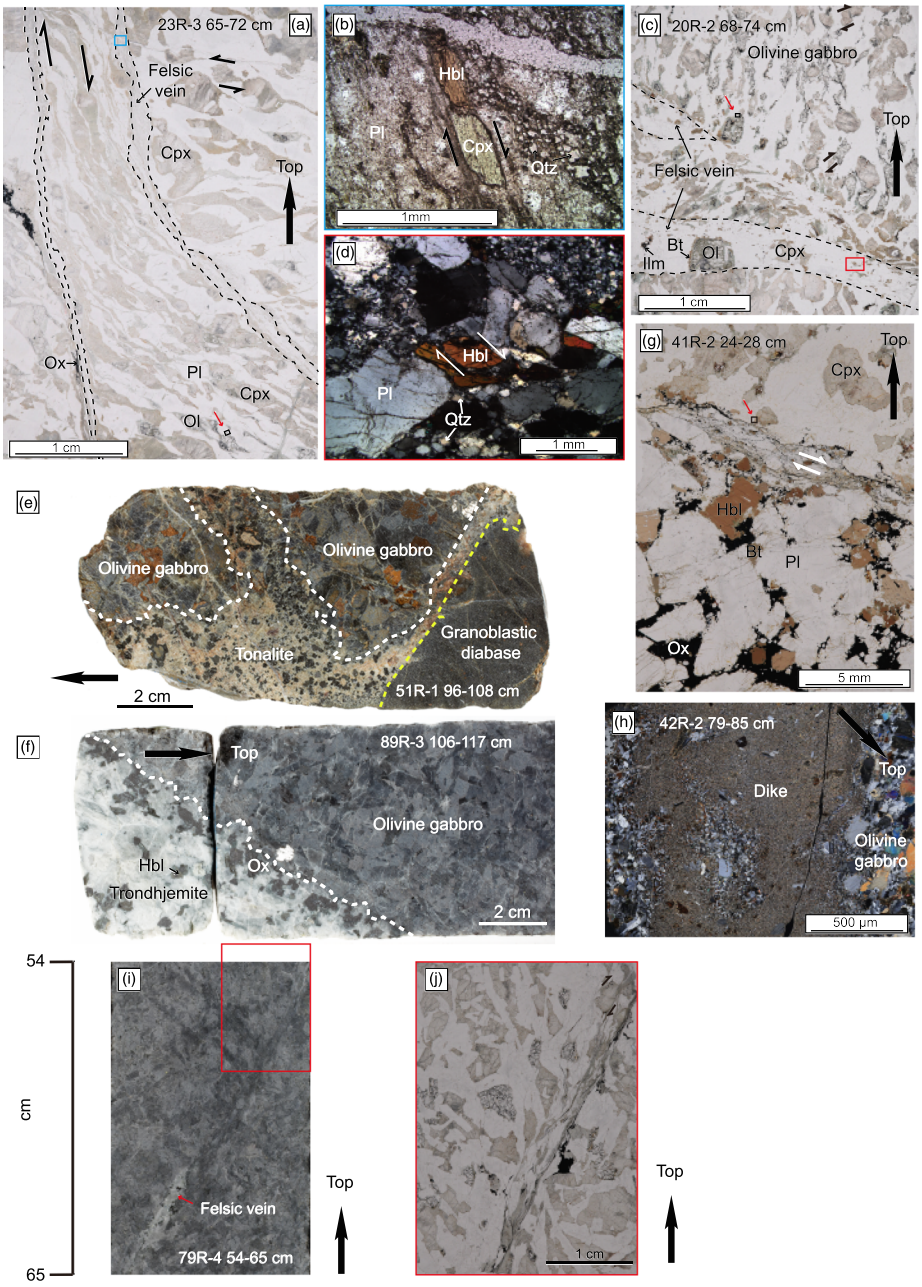

Figure 4. Photomicrographs and core images showing felsic vein occurrences and their relationship to the host gabbros. Sections a, b, c, and g in plane-polarized light, and sections d and h in cross-polarized light. (a) Felsic veins lying along the margin of a normal-sense shear zone crosscutting a reverse-sense sheared olivine gabbro. Blue box shows area of section b. (b) Clinopyroxene fish showing normal shear sense. (c) Normal-sense sheared felsic vein enclosing gabbro relics crosscut a reverse-sense foliated olivine gabbro. Ilmenite and biotite as accessory phases occur in veined gabbro, where ilmenite is the only oxide phase. Red box shows area of section d. (d) Hornblende fish, indicating normal-shear sense, together with undeformed large plagioclase, were enclosed in a veined matrix of plagioclase and quartz neoblasts. (e) Large tonalite patch in hydrated olivine gabbro in contact with granoblastic diabase. (f) Undeformed trondhjemite vein with coarse-grained oxides precipitated along a sutured contact with olivine gabbro. (g) A felsic vein occurs in olivine gabbro with hornblende enclosing plagioclase and a normal-sense sheared contact. (h) Undeformed very fine grained dike apophysis intruding, assimilating, and stopping crystal-plastically deformed olivine gabbro. (i) A sheared flesic vein lies parallel to a reverse-sense sheared oxide gabbro mylonite, where shear sense indicator is shown in zoom-in picture (j). The felsic vein exhibit diffused boundary with respect to the host gabbro. Black rectangles and red arrows in sections a, c, and g correspond to reflected light images c, d, and b, respectively in Figure 8. Large black arrows point to the top of the core. Letter symbols correspond to the following: Ol, olivine; Cpx, clinopyroxene; Opx, orthopyroxene; Pl, plagioclase; Hbl, hornblende; Qtz, quartz; Ox, oxides; Ilm, ilmentite; Bt, biotite.

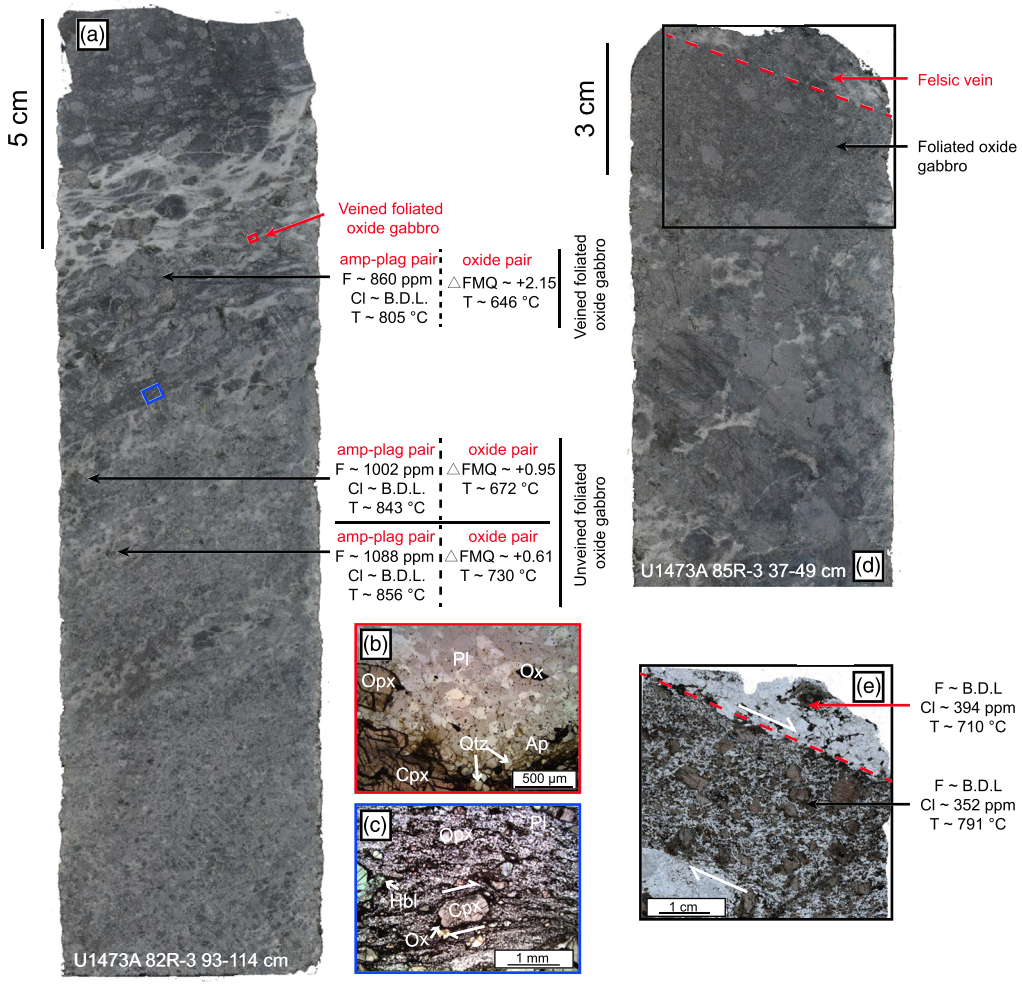

Figure 5. (a) Section image shows gradient of ΔFMQ and temperature measured on oxide pairs, and amphibole-plagioclase equilibrium temperatures including amphibole halogen contents away from a veined reverse shear sense foliated oxide gabbro. Locations of analyzed spots are marked by arrows; (b) and (c) micrographs show the assemblages and shear sense indicator in the adjacent oxide gabbros, carbon-coated thin section under plane light; (d) and (e) hornblende halogen contents and temperatures measured in a weakly deformed felsic vein and adjacent normal shear sense oxide gabbro. B.D.L. stands for "below detection limit." Letter symbols correspond to those in Figure 4.

are similar, both below the detection limit, resulting in similar high Cl/F ratios (Table S6). Moreover, amphibole-plagioclase equilibrium temperature (~769°C) of host gabbro is moderately higher than that (~673°C) of felsic veins. Therefore, we conclude that the formation conditions recorded in the adjacent gabbro are close to that of felsic veins, and applicable to constraining vein formation conditions of our sample suite. Similarly, Nguyen et al. (2018) suggest that formation of felsic rocks from Hole U1473A are in close relation to the temperature conditions of the host gabbros.

4. Results

4.1. Downhole Shear Sense of Felsic Veins and CPFs Within Gabbros

Figure 2a shows normal shear sense dominates above 680 m in Hole 735B in crystal-plastically deformed gabbros, indicative of tensional stresses and overall extension, whereas reverse shear sense, reflecting compressional stresses and local shortening, dominated below those depths. In Hole U1473A, a transition from dominant normal to reverse shear sense also occurs in the gabbro, but at ~50 mbsf, while unlike Hole 735B, numerous normal shear-sense indicators also occur down hole (Figure 2b). Similarly, the shear sense for

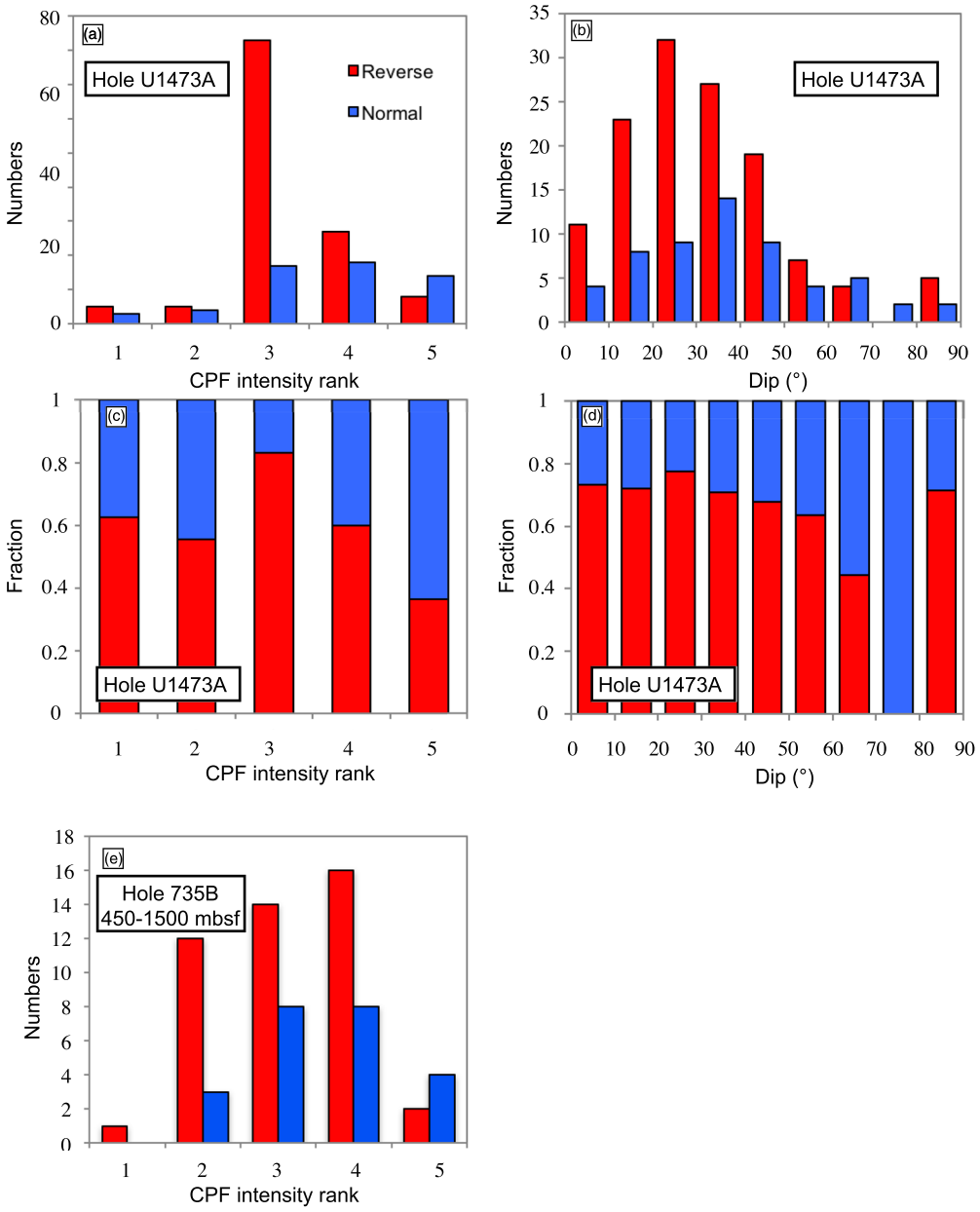

Figure 6. The intensity and dips variation of CPFs with different shear senses in gabbros. (a) and (b) The numbers of CPFs with different shear senses as a function of their intensity rank and dip, Hole U1473A; data are listed in Table S2 in the supporting information. (c) and (d) The relative fraction of CPFs with different shear senses as a function of their intensity rank and dip, Hole U1473A; (e) the numbers of CPFs with different shear senses as a function of their intensity rank, 450–1,500 mbsf of Hole 735B. Data are available at http://www-odp.tamu.edu/publications/176_IR/SUPP_MAT/APPENDIX/. Only CPFs with sense of shear that can be determined are included in these figures. No data are collected from above 450 mbsf of Hole 735B.

felsic veins also shows a transition from normal to reverse at depth of ~640 mbsf in Hole U1473A, where normal shear sense dominates above this depth (Figure 2c).

4.2. CPF Intensity and Dip Variations Within Gabbros

Gabbro CPF intensities from Hole U1473A largely range from protomylonite to ultramylonite (Rank 3 to 5, Figure 6a) where shear sense could be determined. The deformation intensity of reverse-sense CPF's, however, spike at Rank 3, and then sharply decrease as a fraction of normal and reverse sense shear indicators with increasing rank. While normal shear-sense CPFs are less abundant (Figure 6c), they are more evenly distributed from Rank 3 to 5 (Figure 6a). For comparison, deformation intensity of reverse-sense CPFs

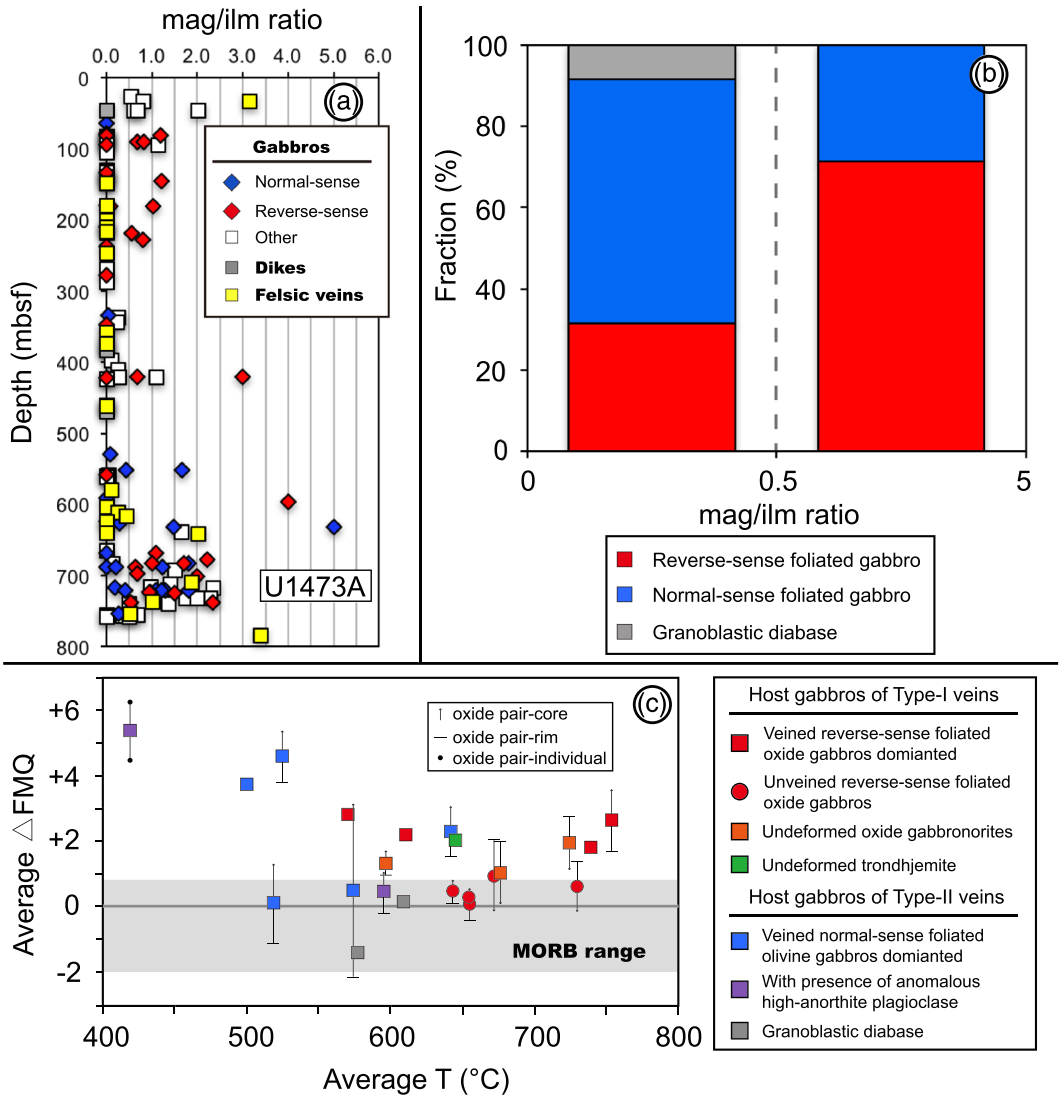

Figure 7. (a) Downhole titanomagnetite-ilmenite ratios in Hole U1473A gabbros. Data are presented in Table S7. (b) Proportions of normal and reverse shear-sense-foliated gabbros with magnetite/Ilmenite ratios less than and greater than 0.5. (c) Average ΔFMQ and equilibrium temperatures calculated from oxide pairs at a given pressure of 1 kbar. The gray box shows the range of MORB oxidation states. Data are listed in Table S4.

from 450–1,500 mbsf of Hole 735B are largely distributed within the range of rank from 2 to 4 (Figure 6e). Similar to normal-sense CPF's in Hole U1473A, normal-sense CPFs from Hole 735B are skewed to higher-intensity rank from 3 to 5 (Figure 6e). At the same time, the dominant CPF dips also differ, with reverse sense foliations slightly shallower (10–40°) than normal shear sense (20–50°), while the proportion of normal and reverse shear-sense foliations is more even overall (Figures 6b and 6d).

4.3. Felsic Veins Occurrence and Mineral Assemblages in Their Host Gabbros

The reverse shear-sense felsic veins (Type I) are associated with oxide gabbro. These veins are crystal-plastically deformed, and generally lie subparallel to the foliation plane in reversely sheared gabbro (Figures 5a, 5c, 4i, and 4j). They generally have irregular or diffused boundary relationship with respect to the host gabbro (Table S1). The host oxide gabbros contain plagioclase + augite + primary hypersthene + titanomagnetite + ilmenite + interstitial or replacive brown hornblende + apatite ± quartz ± zircon (Figures 5b and 5c). Notably, titanomagnetite is relatively abundant, resulting in titanomagnetite/ilmenite ratios of >0.5, which is higher than that of oxides in the hosting gabbro of Type II felsic veins (Figure 7b).

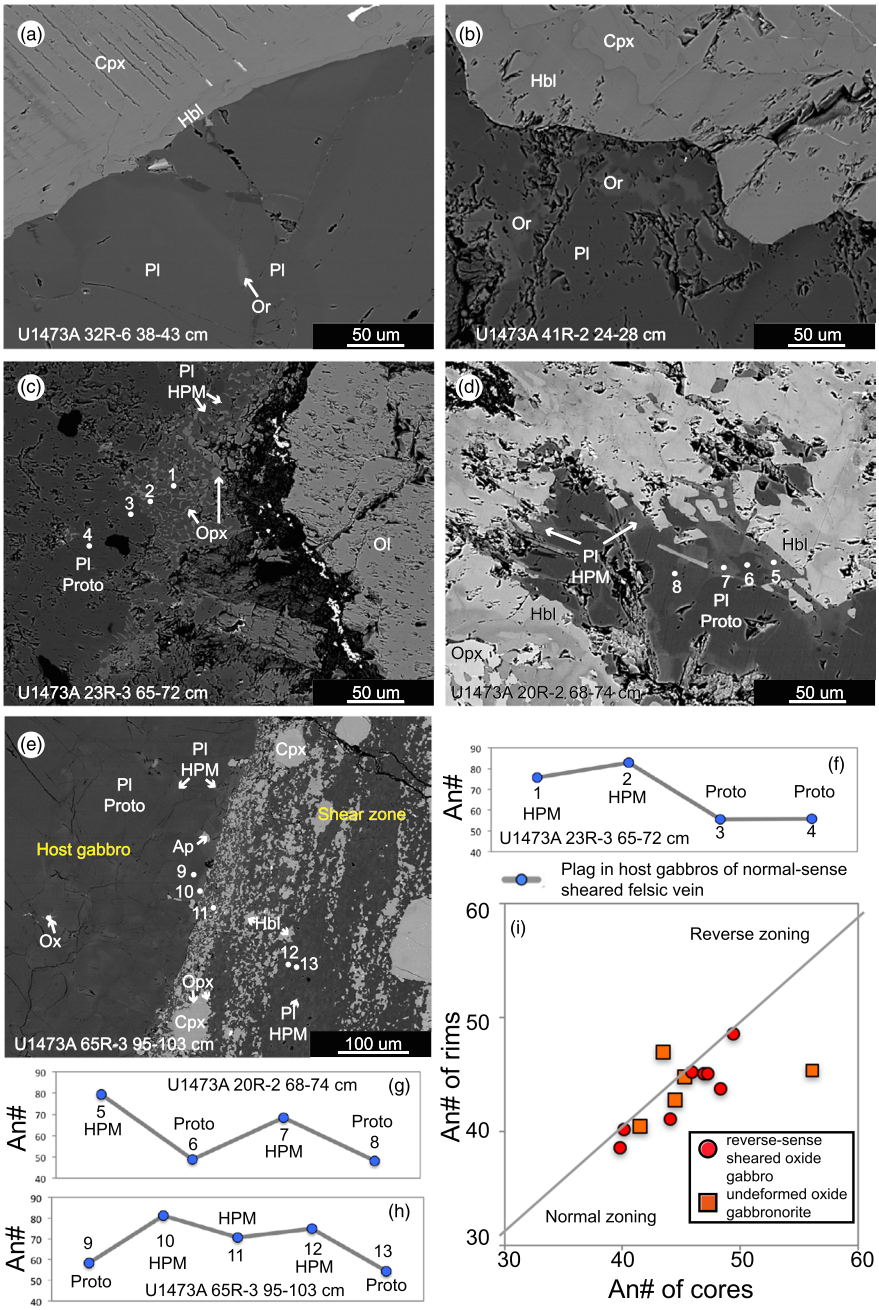

Figure 8. Evidence for hydrous melting in backscatter electron images of gabbros hosting felsic veins and the corresponding plagioclase compositions. (a) Orthoclase in olivine gabbro hosting a felsic vein formed on the margin of a granoblastic dike. (b) Orthoclase in host gabbro of a normal shear-sense felsic vein. (c) Symplectitic intergrowth of anorthitic plagioclase and Opx generated by hydrous partial melting in olivine gabbro hosting a normal-sense sheared felsic vein. (d) Anorthitic plagioclase along the grain boundaries of a primary plagioclase in an olivine gabbro hosting a normal shear-sense sheared felsic vein. (e) Hydrous partial melting-related anorthitic plagioclase in a normal sense shear zone without a felsic vein present. (f, g, h) Plagioclase anorthite content profiles for sections c, d, and e, respectively as indicated by corresponding numbered points. (i) Anorthite content of plagioclase cores and rims in reverse-sense-sheared oxide gabbros including those hosting type I veins. Mineral abbreviations as in Figure 4, with HPM for hydrous partial melting and Ap for apatite.

The Type II felsic veins are generally weak or undeformed and lie along the contact of normal-sense shear zones in olivine gabbro (Figures 4a, 4c, and 4g), and in one oxide gabbro (Figures 5d and 5e). Their host gabbro assemblages may contain titanite, biotite, and orthoclase (Figures 4a and 8b), but have less titanomagnetite and hypersthene, and more ilmenite, which may be present as the only oxide phase. At the same time, brown hornblende often replaces pyroxene in the wall rock hosting Type II veins (Figures 4a, 4c,

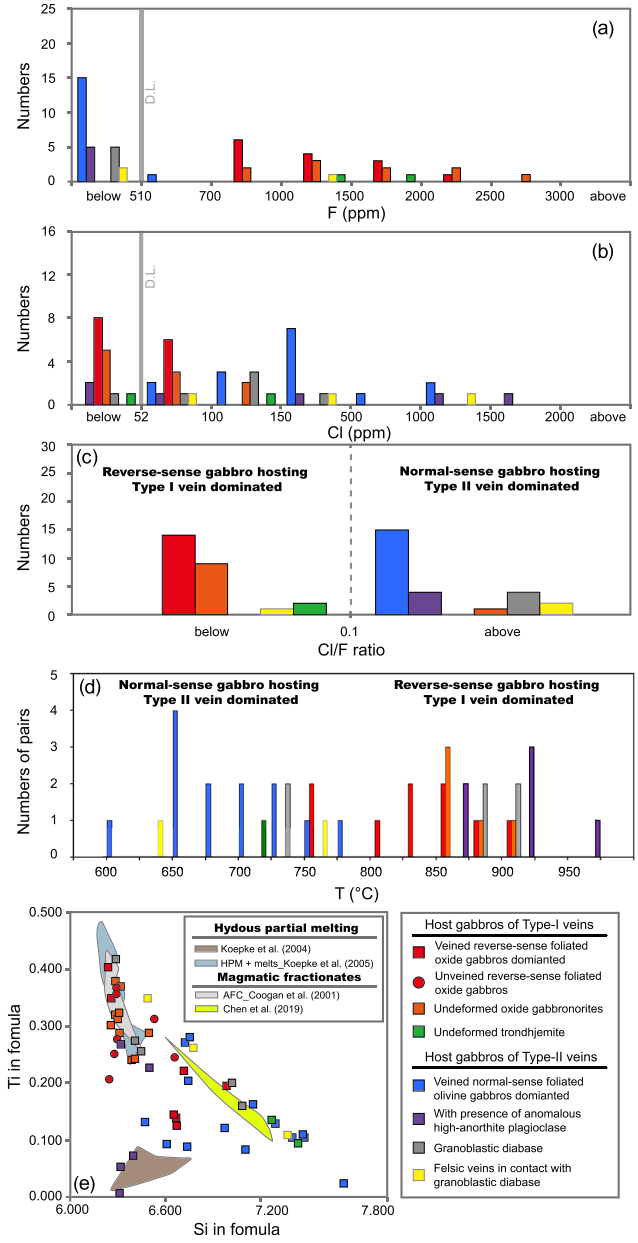

Figure 9. Amphibole compositions and amphibole-plagioclase equilibrium temperatures. Panels (a) and (b) show the F and Cl concentrations of amphiboles, respectively. (c) Gabbros hosting two types of veins are characterized by amphibole Cl/F ratio of 0.1 (gray dash line). The legend is displayed on the right of panel (e). (d) Amphibole–plagioclase equilibrium temperatures calculated at 1 kbar. (e) Comparison of amphibole Ti in formula with those generated by hydrous partial melting (Koepke et al., 2004, 2005) of oceanic gabbros at Atlantis Bank and MARK area. Magmatic amphiboles in MARK gabbros (Coogan et al., 2001) and in Atlantis Bank plagiogranites (Chen et al., 2019) are also included. D. L. stands for "detection limit."

and 4g). Undeformed felsic veins occurring along the margins of dikes have similar mineral assemblages (Figure 8a), but irregular or diffused boundaries relative to the host gabbro (Figure 4e). Two trondhjemite veins from the lower part of Hole U1473A also show diffused vein-gabbro boundaries (Figure 4f), where replacement of clinopyroxene by brown hornblende are observed at the contact.

4.4. Hornblende and Plagioclase Composition, and Their Equilibrium Temperatures

4.4.1. Hornblende and Plagioclase Compositions

Hornblende F, Cl, and Ti contents in foliated gabbros (sensu lato) with opposing shear sense differ significantly, with reverse having low Cl/F, and normal having high Cl/F (Figures 9c and 9e). Gabbros hosting Type I veins, and the unveined reverse shear-sense oxide gabbros, as well as undeformed oxide gabbronorites below 680 mbsf (with one exception) contain low Cl (<100 ppm), mostly below the ~52 ppm detection limit. Correspondingly, they have high F (>700 ppm), and low Cl/F ratios <0.1 (Figures 9a and 9c). At the same time, the vast majority of plagioclase in these oxide gabbros shows normal zoning with more albite-rich rims (Figure 8i).

Nearly all Type II felsic veins occur above 620 mbsf hosted by olivine gabbro, with one oxide gabbro-hosted Type II vein from below 700 mbsf. They generally have high Cl concentrations >100 ppm and low F < 700 ppm, mostly below the ~510 ppm detection limit (Figures 9a and 9b). The hornblende Cl/F ratios in this suite are high (>0.1), and similar to those in the granoblastic hornfels dikes (Figure 9c), whereas the Ti contents are generally lower than those hosting the Type I felsic veins (Figure 9e). In addition, zones of anomalously anorthite-rich plagioclase, suggesting the presence of excess water, are present in two of these host gabbros (Figures 8c and 8d) and in one normal-sense shear zone without felsic veins (Figure 8e, Table S5). The anomalous plagioclase has ~16% to 31% higher anorthite content than adjacent primary plagioclase (Figures 8f, 8g, and 8h), as also observed by Koepke et al. (2005) in the 23°N MAR MARK gabbros.

4.4.2. Amphibole-Plagioclase Equilibrium Temperatures

As shown in Figure 9d, all but one of the amphibole-plagioclase temperatures of the reverse-shear-sense oxide gabbros associated with Type I veins below 640 mbsf and undeformed oxide gabbronorites range from 800–900°C. However, the normal-shear-sense gabbros from above 600 mbsf associated with the Type II veins equilibrated at lower temperatures between 600°C and 800°C. An exception is amphibole equilibrated with the high-anorthite plagioclase rims and patches. These equilibrated at even higher temperatures (850–960°C) than those associated with the Type I veins, but similar to the temperatures (875–925°C) calculated for the granoblastic hornfels dikes (Table S6).

4.5. ΔFMQ, Titanomagnetite-Ilmenite Ratio, and Their Geothermometry

The reverse-shear-sense oxide gabbros associated with Type I veins, and some undeformed oxide gabbronorites, mostly lie within a restricted range of average **Δ**FMQ from 0 to +2.8, with veined oxide gabbros equilibrating, at the higher end (Figure 7c). They generally have a higher titanomagnetite-ilmenite ratio >0.5 (Figure 7b), and their oxide temperatures mainly range from 600°C to 760°C. However, the normal shear-sense gabbros associated with the Type II veins have a highly variable range from ΔFMQ 0 to +5.4 and low titanomagnetite-ilmenite ratio

<0.5 with oxide temperatures mostly lower than 580°C (Figure 7). While these are closure temperatures, and one might interpret the higher temperatures to indicate faster cooling rates, this is unlikely, given the agreement with plagioclase-amphibole temperatures. Thus, the lower ilmenite-titanomagnetite temperatures likely reflect the influence of hydrothermal fluids which allowed recrystallization to lower temperatures, as reflected in their plagioclase-amphibole temperatures as well. Gabbros and felsic veins below 630 mbsf in Hole U1473A have relatively high titanomagnetite-ilmenite ratios, mostly of 0.5–2.5 (Figure 7a), while those above this depth generally have ratios lower than 0.5. Nevertheless, a few samples within depth interval of 25–230 mbsf have moderately high titanomagnetite-ilmenite ratios of 0.5–1.5 (see details in Table S7).

5. Discussion

5.1. Introduction

Nguyen et al. (2018) described seven U1473A felsic veins, dividing them into three types. Veins with sharp boundaries (Type S); veins that pseudomorph the gabbro texture (Type R); and a felsic vein network with diffuse boundaries (Type D). S-Type veins have sharp chemical and textural boundaries with the host gabbro or olivine gabbro, and consist of plagioclase and amphibole, with $An_{2–40}$ sodic plagioclase compared to ~$An_{52–59}$ in the gabbro. The one D-Type consists of a network of veins with irregular curved boundaries that intrudes the host gabbro. There is a relatively narrow compositional gap between host and vein plagioclase (An_{41} vs. An_{31}) and an abundance of apatite and Fe-Ti oxides in the veins. R-Type veins pseudomorph the preexisting texture of the host olivine gabbro, with a large compositional gap to more sodic plagioclase ($An_{>50}$ vs. $An_{<20}$) but the same magnesian pyroxene composition (Cpx Mg# > 80). These were not included in our study. The D-Type vein clearly belongs to our Type I category, while the S-Type represents intrusion of highly evolved melt into subsolidus gabbro via crack networks in the host. Nguyen et al. (2018) conclude that their felsic veins were derived from MORB by a fractional crystallization-dominated process, but after crystallization they acted as channels for hydrothermal fluid infiltration that obscured their magmatic origin.

Dick, Meyer, et al. (1991), relogged Hole 735B and found 0.65 vol.% felsic and 0.43 vol.% intrusive trondhjemite veins. They found that the latter included modified igneous trondhjemites and many of ambiguous paragenesis: some problematically igneous, some clearly hydrothermal. They saw a complete gradation between different kinds of felsic veins, in part because of ongoing, and often extensive, late hydrothermal alteration and overprinting of earlier veins. Thus, positive identification of and discrimination between hydrothermal and late-magmatic origins for many veins is difficult. Of note, a ptygmatically folded zircon-bearing trondhjemite vein in amphibole gneiss at ~27 mbsf suggested an anatectic origin to Dick et al. (1992), and thus a possible example of our Type II veins.

Based on zircon compositions, however, Pietranik et al. (2017) found two generations of felsic veins, one produced by hydrous partial melting in the upper 500 m of Hole 735B, and below 500 m, an older magmatic generation related to the oxide gabbros. These correspond to our Types II and I veins, respectively. Chen et al. (2019), however, concluded that all the felsic veins in Hole 735B formed magmatically by fractional crystallization. Their sample set consisted of 21 veins, with none from the upper 500 m of Hole 735B. Normal shear-sense zones are conspicuously rare below 700 m, from where most of their samples were taken, and abundant above that level, which indicates that their sample set was likely not representative of all the felsic veins in Hole 735B. There are over 400 felsic veins spanning a wide range of compositions and origins in Hole U1473A (MacLeod et al., 2017a) and a similar population in Hole 735B (Dick, Meyer, et al., 1991). It is reasonable that the veins in the two holes represent the similar processes and events as they are only 2 km apart, lie within a single massive gabbro body, and comparisons of the two found that they are very similar (Dick, Kvassnes, et al., 2019). Thus, we conclude that there are at least three distinct vein populations in the two holes including late magmatic fractionates, replacement, and anatectic.

5.2. Origin of Fluids: Magmatic and Seawater-Derived Volatiles

The brown hornblendes in the reverse-shear-sense-foliated oxide gabbros hosting the Type I felsic veins have low Cl/F ratios and high Ti contents (Figure 9). This indicates a deuteric fluid source (e.g., Coogan et al., 2001; Kendrick, 2019; Tribuzio et al., 2000), since the involvement of seawater-derived fluids would result in strong Cl enrichment (Michael & Schilling, 1989). The U1473A equilibrium hornblende temperatures (>800°; Figure 9d) are close to the average temperature (860° ± 30°C) for interstitial amphibole–

plagioclase pairs in MARK ODP Hole 923A and Alvin Dive gabbros (Coogan et al., 2001). These MARK gabbros represent products of assimilation-fractional crystallization by an evolving hydrous silicate melt relatively rich in deuteric volatiles.

We observe high Cl/F ratios in our Type II veins and host gabbros consistent with a seawater-derived origin (Coogan et al., 2001). Koepke et al. (2005) studied gabbros from Holes 920 to 923A and reported compositions of interstitial pargasites, mainly in olivine gabbros drilled above 70 mbsf, coexisting with anomalous anorthite-rich secondary plagioclase. These observations were matched by a series of melting experiments on altered gabbros that produced the same pargasites and high-anorthite plagioclase (Koepke et al., 2004). We note that Koepke et al.'s MARK gabbros have low Cl/F ratios unlike our Type II veins. However, the pargasite in Koepke et al.'s gabbros have high Ti contents, evidence that the fluids had reacted with Fe-Ti oxides as well as plagioclase and clinopyroxene. Thus, they explain their anomalous high-anorthite plagioclase, as products of anatexis induced by seawater-derived fluids at 900–1,000°C, but then modified by Ti-rich melts. This would be consistent with a subsequent nearby oxide-gabbro intrusion.

On the other hand, alteration by seawater-derived fluids can obscure a gabbro's primary magmatic origin, altering the mineralogy, and replacing one amphibole with another (Gillis & Meyer, 2001). This is most easily observed where green amphibole is partially replacing or nucleating on brown hornblende in abyssal gabbros. Thus, we interpret a few relatively low-Ti hornblendes as primarily magmatic as they retain low Cl/F. For example, in sample U1473A 84-1, 52–56 cm an amphibole nucleated on augite at an olivine gabbro-trondhjemite contact grew into the undeformed cross-cutting igneous trondhjemite vein. The low ~708°C plagioclase-brown hornblende temperature indicates post crystallization modification by alteration, but the low Cl/F ratios is consistent with the magmatic origin of the trondhjemites (Figure 9c), which mostly occur below ~500 mbsf in the hole (MacLeod, et al., 2017a).

5.3. Oxidation State

Precipitation of Fe-Ti oxides generally leads to a rapid increase in melt SiO_2 (Berndt et al., 2005; Feig et al., 2006; Koepke et al., 2018; Toplis & Carroll, 1995), which closely relates to the melt oxidation state. This in turn relates directly to the formation of magmatic felsic veins. Reverse-sense-sheared oxide gabbros, including those with Type I veins, generally contain considerable titanomagnetite, with high titanomagnetite-ilmenite ratios, generally >0.5 (Figure 7b). Based on experimental studies, magnetite saturation is favored by high oxidation states from **Δ**FMQ 0 to +4.2 (Berndt et al., 2005; Koepke et al., 2018; Toplis & Carroll, 1995). This is consistent with our observation that **Δ**FMQ in reverse-sense-sheared oxide gabbros with abundant titanomagnetite ranges from 0 to +2.8 (Figure 7c).

Olivine gabbros with normal shear sense and Type II veins generally have titanomagnetite-ilmenite ratios <0.5 (Figure 7b). Saturation of ilmenite in melts is strongly controlled by melt TiO_2 content (Berndt et al., 2005; Toplis & Carroll, 1995). Fe-Ti oxides in normal-sense sheared gabbros, then, including those with Type II veins, have high **Δ**FMQ values, but with a larger range (0 to +5.4) than the oxide gabbros (Figure 7c). This range indicates those olivine gabbros with low titanomagnetite-ilmenite ratios, seemingly contradictory for a parent magma with less TiO_2, is the result of other processes. Natland et al. (1991), for instance, observed growth of ilmenite at the expense of titanomagnetite during recrystallization of oxide gabbro, suggesting the presence of hydrothermal fluids. Consistent with this, ilmenite replaces titanomagnetite in one of our amphibolites (U1473A 10R-1,128–131 cm). Thus, with lower equilibrium temperatures and highly variable oxidation states (Figure 7), we postulate that seawater-derived fluids have significantly modified oxides in normal-sense shear gabbros, consistent with their high Cl/F amphiboles. It is not surprising that the effects of pervasive seawater circulation on the magnetite/ilmenite ratio are more clearly evident in olivine gabbros with low oxide abundance than gabbros with large amounts of oxides.

Granoblastic hornfels diabase also has low titanomagnetite-ilmenite ratios (Figure 7b), which might seem contradictory to the previous conclusion. However, diabase generally has a high proportion of modal oxides, and due to the low oxidation state of MORB melts this is generally largely ilmenite, and the oxidation state indicated by the oxides is within the normal MORB range (ΔFMQ −2 to +0.78, Carmichael & Ghiorso, 1986; Christie et al., 1986). Their high amphibole Cl/F ratios and low oxide equilibrium temperatures, however, clearly reflect the influence of the seawater-derived volatiles in the host gabbros.

Berndt et al. (2005) demonstrated that precipitation of magnetite is nearly independent of melt H_2O contents. Nevertheless, increasing melt H_2O concentration can lead to an increase in fO_2, which in turn results in the formation of magnetite (Zimmer et al., 2010). Thus, oxidizing conditions can be achieved due to processes enriching H_2O such as (1) assimilation of hydrated crust (Juster et al., 1989); (2) an oxidized seawater-derived fluid overprint; (3) enrichment of incompatible magmatic H_2O by fractional crystallization, melt-rock reaction through assimilation fractional crystallization (Dick, Kvassnes, et al., 2019), or reactive porous flow (Lissenberg & MacLeod, 2016). At the Galapagos Spreading Center, for example, the fO_2 of Fe-Ti rich basalts extended up to **Δ**FMQ +3 due to assimilation of oxidized crust, leading to early precipitation of magnetite (Juster et al., 1989). However, in this case, Fe-Ti melts should show chlorine overenrichment (Michael & Schilling, 1989), and result in the formation of high Cl/F ratio hornblendes. However, the U1473A gabbros hosting the Type I veins are not the product of such melts. The magmatic hornblendes, high oxide-equilibrium temperatures and relatively restricted oxidation state range of the U1473A oxide gabbros show that the influence of overprinting of seawater-derived fluids is limited, unlike in the normal-sense sheared gabbros. Thus, we speculate that the high **Δ**FMQ of reverse-sense-sheared oxide gabbros are reasonably the result of H_2O enrichment during magmatic processes such as fractional crystallization, assimilation fractional crystallization, or reactive porous flow.

5.4. Felsic Vein Petrogenesis: Implications From Their Host Gabbros

5.4.1. Type I Veins: Simple Fractional Crystallization or Liquid Immiscibility?

Extreme fractionation of melts has been postulated to produce felsic veins by liquid immiscibility along with a Fe-Ti-rich melt. Whether this has occurred at Atlantis Bank has been hotly debated and depends on when oxide saturation occurs; early onset would prevent the necessary iron enrichment. The onset of magnetite precipitation occurs at or near NNO buffer, and leads to strong silica enrichment in a melt (Berndt et al., 2005; Juster et al., 1989; Toplis & Carroll, 1995). Several experimental studies of MORB differentiation show that high H_2O and ΔFMQ stabilizes orthopyroxene and magnetite (Berndt et al., 2005; Feig et al., 2006; Juster et al., 1989). This is consistent with the greater abundance of titanomagnetite resulting in high titanomagnetite/ilmenite ratios >0.5, and the common presence of orthopyroxene in Hole U1473A reverse-sense-sheared oxide gabbros relative to normal-sense sheared gabbros (Figure 7b). Magmatic brown hornblende is also present in all our reverse-sense-sheared oxide gabbros, indicative of high water activity (Koepke et al., 2018). Koepke et al. (2018), based on experiments, proposed that Atlantis Bank oxide gabbros can be produced under variable water activity ($aH_2O = 0.1–1$) and redox conditions (ΔFMQ −1.1 to +3.2). Magmatic amphiboles can be stabilized by H_2O enrichment after ~90–95% simple fractional crystallization of a basalt with ~0.2 wt.% H_2O following the end of oxide gabbronorite crystallization based on modeling results (Gillis & Meyer, 2001).

The situation, however, is a bit more complex as normal zoning of plagioclase in reverse-sense-sheared oxide gabbros (Figure 8i) are in accordance with both assimilation fractional crystallization (Coogan et al., 2001; Dick, Kvassnes, et al., 2019; Gao et al., 2007) and reactive porous flow models (Lissenberg & MacLeod, 2016) involving in melt-rock reactions. At the same time, these two models result in overenrichment of incompatible elements in the melts (Dick, Kvassnes, et al., 2019; Gao et al., 2007; Lissenberg & MacLeod, 2016), and H_2O as well due to its incompatible behavior. As a result, this may lead to the increasing fO_2 resulting in the earlier precipitation of titanomagnetite. Thus, the actual percent crystallization of felsic veins may be lower due to uptake of incompatible water from preexisting cumulates. The anorthite content of plagioclase in Type I veins and plagioclase rims in the veined reverse-sense-sheared oxide gabbros range from ~34 to 45 (Table S5). Based on MELTS modeling for fractional crystallization of primary MORB matching Hole 735B bulk compositions with assumed 0.15 wt.% H_2O (Lissenberg & MacLeod, 2016), silica-rich melts producing these plagioclases correspond to ~86% to 91% crystallization of a primitive MORB melt. Similarly, Niu et al. (2002) proposed that felsic veins can form at 85% to 90% fractionation of a primitive MORB by determining the liquid line of descent defined by Hole 735B gabbros and felsic vein compositions. With this crystallization degree, melt H_2O concentrations would be lower than 2 wt.%, which cannot stabilize magmatic amphibole (see Gillis & Meyer, 2001). This is in contrast to the common presence of brown hornblende in magmatic felsic veins, which in turn suggests H_2O overenrichment occurs due to melt-rock reaction in the Atlantis Bank gabbros and felsic veins.

The normal plagioclase zoning in Type I veined oxide gabbros and in plagioclase in an oxide-bearing gabbro hosting Vein-D (hybridized gabbro-felsic vein with diffused boundary) from Hole U1473A (Nguyen et al., 2018) suggest that melt-rock reactions have occurred (Figure 8i). Koepke et al. (2018) estimate that the solidus temperatures of oxide gabbro can be as low as ~800°C under water-saturated conditions. High amphibole–plagioclase equilibrium temperatures (>800°C) of reverse-sense oxide gabbro hosting Type I veins indicate that they might not be fully solidified during vein formation. This is consistent with the irregular or diffused vein-gabbro boundaries in our samples (Figure 4i and Table S1), and that between Nguyen et al.'s (2018) Hole U1473A apatite- (10%) and oxide- (15%) rich "Vein-D" diorite and its host oxide gabbro. This is indicative of similar temperature conditions, which they proposed represent the earliest stage of SiO_2-rich melts.

The often intimate coexistence of felsic veins with oxide gabbros from the upper 500 m of Hole 735B might imply a mixture of Fe-rich melts and siliceous melts that separated immiscibly (Natland et al., 1991). Their fO_2 is generally close to the QFM buffer, and all are below the NNO buffer. Experimental studies show that these oxidation states are too low to stabilize magnetite, whereas ilmenite, mainly controlled by melt TiO_2, may saturate (Berndt et al., 2005; Juster et al., 1989; Toplis & Carroll, 1995). Even with ilmenite saturation, ferrobasalt melts may continue iron enrichment up to ~18 wt.% FeO (Toplis & Carroll, 1995). Dixon and Rutherford (1979) demonstrated experimentally that silicic melts and Fe-rich melts (FeO ~ 20 wt.%) formed immiscibly after 95% crystallization of primitive anhydrous basalt at ~1,010–1,040°C at 1 atm and below NNO buffer.

However, crystallization experiments performed by Koepke et al. (2018) demonstrate that 735B oxide gabbros formed under wetter conditions, where liquid immiscibility cannot be attained. As discussed above, with even earlier oxide precipitation due to melt-rock reaction and assimilation of incompatible water, the oxygen fugacity would be high. The common presence of amphiboles and orthopyroxene, and more abundant titanomagnetite in oxide gabbros indicates high water activity and oxidizing conditions during their formation (Berndt et al., 2005; Feig et al., 2006; Koepke et al., 2018), which would not favor liquid immiscibility. In addition, much higher Ca/Na ratio compared to the silicate melts characterizes Fe-rich melts (Dixon & Rutherford, 1979), which should produce reverse zoning in the oxide gabbro plagioclase. Thus, the normal zoning, and the high ΔFMQ, in the reverse-sense-sheared oxide gabbros hosting Type I veins cannot be due to liquid immiscibility, which would require relatively low fO_2 to reach the required extreme iron enrichment. Therefore, we conclude that Type I veins are the fractionates following oxide precipitation and involving in melt-rock reactions during either assimilation fractional crystallization or reactive porous flows.

5.4.2. Type II Veins: Evidence for Hydrous Partial Melting

In the normal-shear-sense foliated gabbros hosting Type II veins, replacive hornblende has low TiO_2 but high Cl/F >0.1 (Figures 9c and 9e). These compositions indicate that seawater volatiles are involved in their formation (Coogan et al., 2001), consistent with their generally lower equilibrium temperatures 650–800°C (Figure 9d). Independently, the temperatures found for deformed gabbros sampled from the seafloor around Atlantis Bank also indicate initiation of hydrous alteration at ~800°C (Miranda & John, 2010). Further, Sanfilippo et al. (2017) reported that U1473A brown amphibole veins with high Cl contents were generated by interaction of seawater-derived fluids with residual melts, which suggests ingress of seawater-volatiles initiated at higher temperature of ~850°C. The presence of anomalous anorthite-enriched plagioclase with orthopyroxene and pargasite are believed characteristic of hydrous gabbro anatexis with the reaction: olivine + clinopyroxene + plagioclase$_1$ + H_2O = orthopyroxene + pargasite + anomalous anorthite-enriched plagioclase + felsic melt (Koepke et al., 2004, 2007). In three of our samples with high Cl/F amphiboles equilibrated with these anomalous high-anorthite plagioclase, we found even higher temperatures, ~850–960°C (Figure 9d): two directly in contact with Type II felsic veins (Figures 4a and 4c), and an additional unveined normal-sense sheared gabbro sampled at ~589 mbsf. This might extend the depth of seawater infiltration to deeper and to higher temperatures; however, it is more likely that this reflects a local spike in temperature in the wall rocks due to dike intrusion and anatexis where seawater circulation had occurred earlier.

High Cl/F ratios (>0.1) hornblende in granoblastic hornfels diabase (Figure 9c) indicates assimilation of seawater-derived volatiles into the diabase as it crystallized. These dikes occur down to 469 m in Hole U1473A, with plagioclase-amphibole temperatures of 875–925°C, providing additional evidence for deep,

higher-temperature circulation of seawater-derived volatiles. With abundant evidence that a sheeted dike complex once overlay the Atlantis Bank gabbros, our results clearly show that seawater was circulating down below the dike-gabbro transition.

In addition, orthoclase appears near the contact of a normal-sense sheared felsic vein in the host rock (Figures 4g and 8b) and at the contact of an anatectic felsic vein generated by diking (Figure 8a). Biotite is also found associated with two of the normal-sense sheared felsic veins (Figures 4c and 4g). Orthoclase is a common differentiation product of calc-alkaline basalt, ut not MORB due to its extremely low K_2O content. Anatexis of the host gabbro and involvement of seawater, however, can lead to enrichment of potassium in the melts and then orthoclase and biotite formation (Ahmed, 1993; Flagler & Spray, 1991). Thus, their presence with high Cl/F ratio amphibole supports an origin by anatexis of the Type II veins.

5.5. Internal Stress Field Change

5.5.1. Origin of the Normal-Sense Shear Zones

The felsic veins and gabbros with different shear sense in Holes 735B and U1473A provide a unique opportunity to examine the evolving internal stress field and fluid circulation during crustal accretion at an asymmetric ultraslow spreading ridge. Figure 2 shows that normal shear sense dominates the crystal-plastically deformed gabbros above 50 m in Hole U1473A, and above 650 m in Hole 735B, indicative of extensional stress, whereas reverse-shear sense reflecting compressional stress dominates below those depths. Though some show weak normal shear sense, most felsic veins found within normal-sense shear zones in gabbro have undergone little or no crystal-plastic deformation (Figures 4d and 4g). Based on our sample set and the cruise report, four samples show clear cross-cutting relationships between shear zones. After applying a rotation of 12° either clockwise or anticlockwise, the cross-cutting relationships of three samples remain unchanged (see section 3.2.3). In two of them, we found a reverse-sense shear zone that was cut by a normal-sense shear zone that contained a normal shear-sense Type II felsic veins (Figures 4a and 4c). With one exception, it shows a veined reverse-sense shear zone cut the reverse-sense foliated gabbro. While it changed to normal-sense shear zone cross-cutting reverse-sense foliated gabbro subsequent to a clockwise rotation of 12° (Table S3). There are no reported cases where reverse-sense shear zones cut normal sense in the gabbros. Based on this, and the conditions of their formation (magmatic vs. anatectic), Type II felsic veins likely postdate the Type I veins and the reverse shear-sense deformation.

Thus, we have a high-temperature magmatic event, followed by lower-temperature anatexis during normal faulting associated with diking, indicating an intervening major change in the stress field. The diking is clearly related to extension across the plate boundary, where fissuring and normal faulting allowed circulation of seawater down into the crust. The Type II anatectic veins, their high Cl/F ratios, and wide range fO_2 clearly indicate that this circulation continues down to at least 800°C based on the temperatures indicated by plagioclase–amphibole thermometry.

5.5.2. Origin of the Reverse-Sense Shear Zones

Reverse shear sense in foliated gabbro dominates below 650 and 50 m in Hole 735B and Hole U1473A, respectively. Normal shear-sense veins hosted by olivine gabbro are far more abundantly higher in Hole U1473A (Figure 2c). The felsic veins with reverse shear sense from Hole U1473A are generally crystal-plastically deformed. The reverse shear sense and its association with late Fe-Ti-rich melts and magmatic felsic veins shows these faults initiated in the final stage of crystallization of the gabbro massif. The higher temperature reverse-shear-sense deformation peaks at a dip between 20° and 30°, whereas the cross-cutting lower-temperature normal-sense deformation peaks between 30° and 40° and falls off more slowly to higher dip angles (Figure 6b). This indicates an evolving stress field. While cooling of a magma to ambient temperature generates 1–2% isotropic dilation with microcracking in the primary igneous phases, by itself this cannot account for reverse sense faults. Paleomagnetic data of Hole 735B, assuming an east-west rotation axis, indicates that the footwall rotated ~20° after the gabbro massif cooled below the Curie temperature (<580°C: Dick et al., 1999; Kikawa & Pariso, 1991). Nevertheless, inclination data from Hole U1473A indicate a smaller tectonic rotation of up to 12° (Morris et al., 2016). These relative tectonic rotations may account for difference in dips, but not the change in shear sense (see section 3.2.3). Assuming the crystal-plastic foliations originally dipped shallowly to the north, this rotation might lead normal-sense shear zones to display reverse sense after rotation, but only for initial dips < ~20° (Dick et al., 1999). This simply cannot explain the wide range of reverse shear-sense dips, which extend to much higher angles

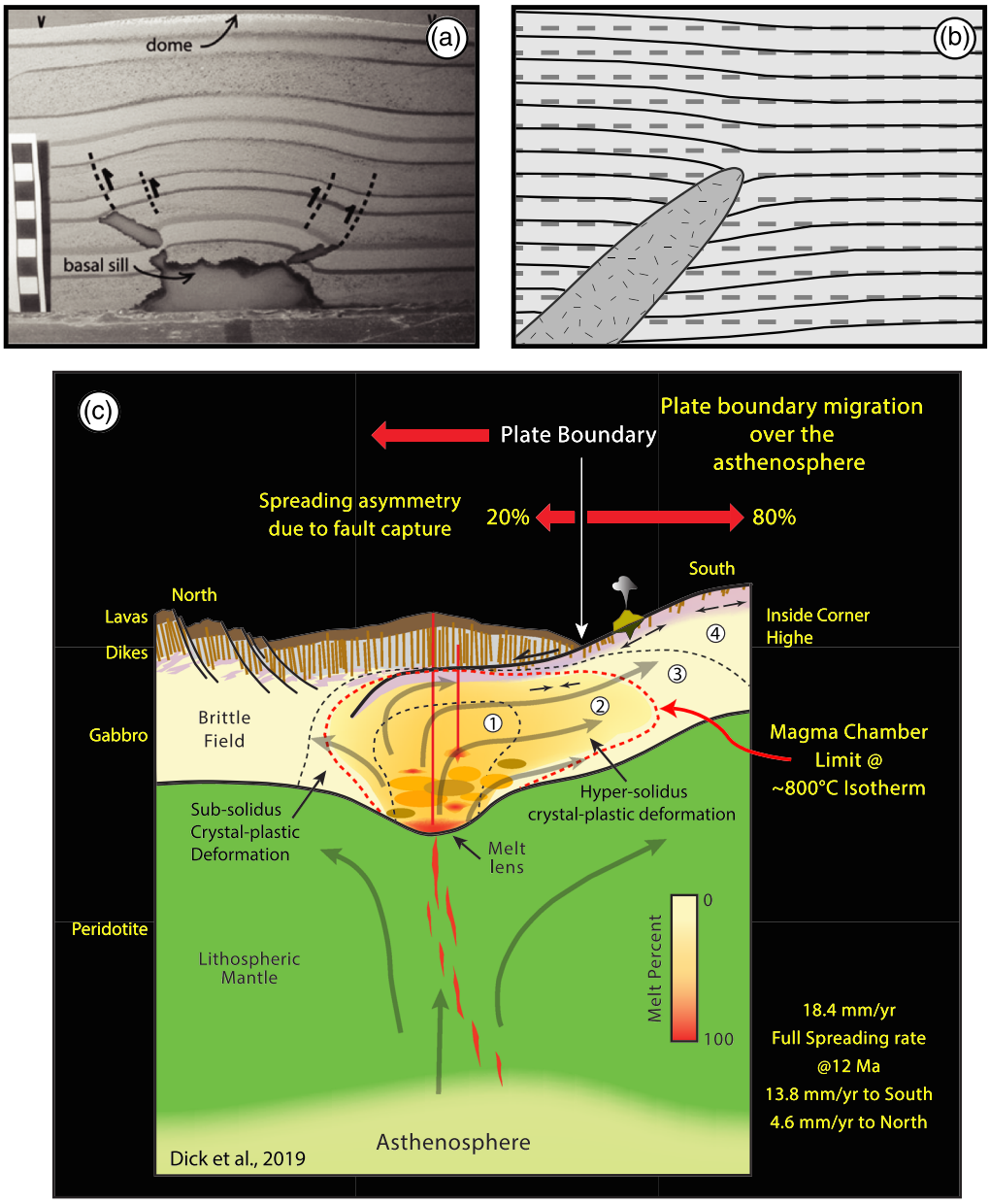

Figure 10. (a) Sketch of an experiment injecting cold honey along the wall of a sand-filled box where a cup-shaped intrusion forms with reverse faulting above it (Mathieu et al., 2008). (b) Mechanical simulation of a dike propagating at 45° to a preexisting planar structure (dash lines) with the displaced positions of the planes shown by the solid lines (Pollard, 1973). The sense of rotation of the layers is consistent with reverse faults forming at the interface between the intrusion and the country, which the authors suggest is a likely analog situation for asymmetric intrusion and spreading during emplacement of the Atlantis Bank OCC. Solid and dash lines show the reverse sense of movement, rather than assuming that host rock is subhorizontal. (c) Cartoon modified from Dick, Kvassnes, et al. (2019) to show the plate migration over the asthenosphere inferred from fault capture and asymmetric spreading for accretion of the lower crust and emplacement of the Atlantis Bank OCC and gabbro batholith. Bathymetric profile is from the present day ridge axis at 57°15′E, 31°50′S (no vertical exaggeration). Deformation zones are numbered in the white circles: Region 1 is inferred crystal mush zone and axis of intrusion; Region 2 is the zone of hypersolidus crystal plastic deformation; Region 3 is the zone of subsolidus high-temperature crystal-plastic deformation; Region 4 is the zone of brittle deformation. Spreading asymmetry is based on the results of Baines et al. (2008).

(Figure 6d). In any case, our preferred fault geometry based on the evidence presented in this paper, and elsewhere (e.g., Dick, Kvassnes, et al., 2019) is a flat-ramp flat, where instead of plunging vertically downward beneath the southern rift valley wall, the detachment fault goes listric and curves to subhorizontal extending across the rift valley along the brittle-ductile transition (Figure 10).

Even with the much larger rotation predicted for a detachment fault that plunges vertically into the axis of upwelling, there is still not enough to produce our steeper reverse-sense shear zones from normal-sense shear zones. Moreover, the gabbro reverse-sense CPFs are skewed to significantly lower intensity while the normal-sense gabbro CPFs are skewed to higher intensities in both Hole U1473A and Hole 735B (Figures 6a and 6e). This indicates that the reverse shear-sense deformation was more broadly distributed, while the normal sense was more localized consistent with shear localization at lower temperatures. Most recently, Deans and Yoshinobu (2019) by reorientating core pieces back to the geographic reference frame suggest that the development of magmatic and high-temperature crystal-plastic foliations in Hole 735B are associated with internal processes beneath detachment footwall, such as magmatic intrusion rather than simple ridge-perpendicular extension.

Our first attempt at explaining the two felsic vein parageneses was based on Parnell-Turner et al.'s (2017) teleseismic study of the 13°20′N core complex. They found two belts of earthquakes at the MAR 13°20′N OCC indicating reverse and normal faulting, respectively. The reverse faulting occurred at depths from 3 to 7 km in a 2-km-wide region offset 3 to 4 km west of the center of the neovolcanic zone below the detachment footwall. A second belt of contemporaneous earthquakes with normal fault solutions was restricted to a narrow 3-km band of seismicity at 7–12-km depth beneath the neovolcanic zone. These faults indicate a geometry based on an elastic bending model where the fault curves smoothly over the compressional earthquakes down into the zone of normal faulting with a maximum dip of ~70°. However, the MAR 13°20′N OCC, with abundant mantle peridotites exposed on the seafloor, has a low magma budget while Atlantis Bank represents the most magmatic known OCC. Thus, we would anticipate that the geothermal gradient would have been much steeper at Atlantis Bank, and the stress distribution would be significantly different. Moreover, the 13°20′N fault sequence is different from that inferred for the Types I and II veins. The reverse faulting is shallower than the normal faulting at 13°20′N, the opposite of what we observe for the Types I and II veins where the Type II veins clearly formed beneath the rift axis due to their association with the dikes, as discussed below, while the Type I veins formed deeper under hypersolidus conditions.

Dick, MacLeod, et al. (2019) show three examples of anatectic veins and incipient melting of the gabbro against dikes at 284, 381, and 459 mbsf. These have brown hornblende that formed at 600° to 775°C, and thus crystallized in the upper amphibolite to granulite facies. Sheeted dikes in IODP Hole 1256D, except at the contact with the melt lens, are all greenschist facies, down to about 1,270 mbsf, rising rapidly in metamorphic grade to granulite facies in the contact aureole with the melt lens (Wilson et al., 2006). Such temperature conditions, in the absence of a melt lens (Dick, MacLeod, et al., 2019), would likely only exist at the bottom of the dike-gabbro transition beneath the rift valley, not several hundred meters below seafloor on the rift valley wall. Thus, the Type I veins formed, in a compressional regime deep below the rift valley axis and not below the hanging wall due to slab bending stresses.

Faulting above dikes is well documented in the field and in the laboratory and, reflecting an extensional environment, produces normal faulting and thinning of the overlying crust. This is consistent with the normal-sense shear zones we observe associated with the anatectic Type II felsic formed during dike injection in the upper crust. However, the stress field around a buoyant crystal mush intrusion deep below the dike-gabbro transition is likely very different than for a vertical dike. One might initially envisage a mushroom shape as the crystal mush rises up and spreads out beneath the dike-gabbro transition. Such an intrusion would produce reverse faulting at its wings and doming up of the overlying rocks as seen in analog experiments with extension across the top of the dome (e.g., Mathieu et al., 2008; Schultz-Ela et al., 1993; Figure 10a). This is consistent with the simple extensional fissuring found across the inner rift valley floor of slow-spreading ridges, where normal faulting is largely confined to the flanks of the inner rift valley (e.g., Karson & Dick, 1983). Another relevant geometry is where an intrusion is deflected to a steep angle and the overlying rocks are pushed upward, while the underlying rocks are displaced downward (Figure 10b; Pollard, 1973). Such an intrusion would produce a stress field around it consistent with reverse faulting. This is likely the case for intrusion of the lower crust where asymmetric spreading occurred 14.1 mm/yr to the south, and 3.1 mm/yr to the north during emplacement of the Atlantis Bank OCC (Baines et al., 2008) at the time of emplacement. While accretion is not happening in a static setting, this would be the case as the partially molten gabbro diapir would be more buoyant than the more solidified gabbro into which it was intruded.

Thus, our preferred interpretation of the Type I and Type II felsic veins and their relationship to the emplacement of the Atlantis Bank Core Complex is shown in Figure 10c (modified from Dick, Kvassnes, et al., 2019). The asymmetric spreading implies a similar asymmetric crystal mush zone consisting of a composite intrusion formed from numerous smaller intrusions. This composite intrusion rises buoyantly up between the diverging tectonic plates, accommodating extension both by magmatic accretion and by crystal-mush flow. As it approaches the solidus, with decreasing melt percentage, crystal-plastic deformation will occur, likely by varying creep mechanisms including grain-boundary sliding, diffusion creep, and dislocation creep (Mehl & Hirth, 2008; Yoshinobu & Hirth, 2002; Zhou et al., 2012) accommodating extension. Fractional crystallization of the late interstitial melt at this point produces the Type I felsic veins, which are later deformed with their host gabbros, as they cool into the solid state and are emplaced into the extensional regime and the dike-gabbro transition. There, the rocks underwent brittle deformation regime, and normal faulting replaces the reverse concurrent with hydrothermal circulation of seawater-derived fluids. Locally weak crystal-plastic deformation is found in some of the Type II veins, demonstrating that the dikes rooted down into the brittle-ductile transition. Local anatectic melting then occurred when dikes were emplaced into hydrated gabbros. Numerous diabase dikes were recovered by dredging and diving around Atlantis Bank, and a total of seven dikes were drilled in Holes 735B and U1473A—none were crystal-plastically deformed and the dikes always crosscut crystal-plastic foliations in the gabbros (Figure 4h; Dick, Kvassnes, et al., 2019).

Region 1 in our model (Figure 10c) is a hypothetical crystal-mush zone, Region 2 is the hypersolidus crystal-plastic deformation zone, Region 3 shows the solidus region that bounds the magma chamber (Regions 1 and 2), while Region 4 is the zone of brittle deformation. The 2–3 boundary is not an isotherm as the solidus temperature varies with depth both due to changing bulk composition and due to melt compaction driving off interstitial melt, leaving refractory residues at the base of the section. At the same time as the interstitial melt is compacted upward, melt-rock reaction and an evolving melt composition results in a much lower solidus temperature (~850°C) at the top of the section. Region 2 is the brittle-ductile boundary, which would jog at the crust-mantle boundary depending on the relative strengths of gabbro and peridotite. As shown, this boundary assumes near constant cooling of the lithosphere with age, and has an asymmetric shape due to the contrasting half spreading rates. It also curves below the sheeted dikes at the brittle-ductile transition. Below the brittle-ductile transition there is a region of reverse faulting that extends through the solidus into the melt present region due to the asymmetric intrusion outlined by the solidus. Region 3, lying above the brittle-ductile transition undergoes extensional stress and includes the uppermost lower crust emplaced mechanically into the dike-gabbro transition, and the limit of seawater circulation. Finally, Region 3, undergoes extension due to slab bending, with circulation of seawater resulting in retrograde metamorphism, first in the granulite facies, then amphibolite facies, on down to ambient temperature near the seafloor.

Our data then strongly support the model implicit in this cartoon, which also answers the question of where the heat source for black smokers and massive sulfide deposits on long-lived detachment faults is located. Fault capture and asymmetric spreading resulted in migration of the plate boundary to the north at the paleo Southwest Indian Ridge (SWIR), as shown in Figure10, such that the rift valley axis overrides the upwelling asthenosphere and skews the crustal isotherms to the south, which then provides the primary heat source driving hydrothermal circulation beneath the core complex. This may also possibly explain the observations of John et al. (2004) and Schwartz et al. (2005) for off-axis intrusive activity implied by zircon dating at Atlantis Bank.

6. Conclusions

Based on our results, we identify two generations of felsic veins that formed sequentially during diapiric intrusion of gabbro to the dike-gabbro transition beneath the SWIR. Type I veins formed by fractional crystallization under a compressional stress regime during diapiric intrusion, associated with generally higher-temperatures (800–900°C) and formation of semibrittle to ductile reverse-sense shear zones. Type II veins are generally related to normal-sense shear zones due to dike intrusion and hydrous melting (anatexis) in hydrothermally altered gabbros. This, and the low magnetite/ilmenite ratios in the olivine gabbros, demonstrates that pervasive seawater circulation occurred at temperatures >800°C down to at least 590 m—the depth of the deepest evidence for hydrous partial melting.

The asymmetric spreading of the crust during emplacement of the core complex provides the most likely explanation for the evolving stress field required to explain the two generations of felsic veins, reflecting internal stresses within an asymmetrically emplaced gabbro diapir. This is a natural consequence where fault capture sequesters the larger portion of the accreting lower crust, which then migrates more rapidly to the south as show in Figure 10c (Dick, Kvassnes, et al., 2019). Finally, the implied asymmetry of intrusion has implications for the source of the heat for massive sulfide deposits on the footwalls of large oceanic core complexes, as the advancing plate boundary overrides the zone of magmatic intrusion as it migrates to the north.

Data Availability Statement

"The data used in this paper can be found in the supporting information and is archived in the PetDB database maintained by the Lamont-Doherty Earth Observatory, Palisades, NY (https://search.earthchem.org/). Additional data used are at this site (http://web.iodp.tamu.edu/OVERVIEW/).

Acknowledgments
This study was supported by the Chinese National Key Basic Research Program (Grant 2012CB417300). H. Dick and B. Urann were supported by U.S. National Science Foundation (Grant OCE-MG_x00026;G 8371300). Emmanuel Codillo provided numerous useful comments and moral support. We thank N. Chatterjee for assistance in analyzing major element mineral composition in the MIT Electron Microprobe Laboratory. The great contributions of 360 Scientific Party for their initial shipboard description and interpretations of the Hole U1473A cores made this work possible. Special thanks go to C. J. MacLeod, Expedition cochief scientist, and Peter Blum, staff scientist, Stephen Midgley, IODP operations superintendent, and Siem Offshore James Samuel McLelland, offshore installation manager, ship's master Terry Skinner, and the crew and drillers on the JOIDES Resolution.

References

Agar, S. M., & Lloyd, G. E. (1997). Deformation of Fe-Ti oxides in gabbroic shear zones from the MARK area. In J. A. Karson, M. Cannat, D. J. Miller, & D. Elthon (Eds.), *Proceedings of the ocean drilling program*, *Scientific Results* (Vol. 153, pp. 123–141). College Station, TX: Ocean Drilling Program.

Ahmed, Z. (1993). *Leucocratic rocks from the Bela ophiolite, Khuzdar District, Pakistan*, *Special Publications* (Vol. 74, pp. 89–100). London: Geological Society. https://doi.org/10.1144/GSL.SP.1993.074.01.07

Andersen, D. J., Lindsley, D. H., & Davidson, P. M. (1993). QUILF: A Pascal program to assess equilibria among Fe-Mg-Mn-Ti oxides, pyroxenes, olivine, and quartz. *Computers & Geosciences*, *19*(9), 1333–1350. https://doi.org/10.1016/0098-3004(93)90033-2

Baines, A. G., Cheadle, M. J., Dick, H. J. B., Hosford, S. A., John, B. E., Kusznir, N. J., & Matsumoto, T. (2003). A mechanism for generating the anomalous uplift of oceanic core-complexes: Atlantis Bank, SW Indian ridge. *Geology*, *31*, 1105–1108. https://doi.org/10.1130/G19829.1

Baines, A. G., Cheadle, M. J., John, B. E., & Schwartz, J. J. (2008). The rate of oceanic detachment faulting at Atlantis Bank, SW Indian ridge. *Earth and Planetary Science Letters*, *273*, 105–114. https://doi.org/10.1016/j.epsl.2008.06.013

Berndt, J., Koepke, J., & Holtz, F. (2005). An experimental investigation of the influence of water and oxygen fugacity on differentiation of MORB at 200 MPa. *Journal of Petrology*, *46*(1), 135–167. https://doi.org/10.1093/petrology/egh066

Blackman, D. K., Ildefonse, B., John, B. E., Ohara, Y., Miller, D. J., MacLeod, C. J., & Scientists, E. (2006). *Proceedings of the Integrated Ocean Drilling Program*. College Station TX: Integrated Ocean Drilling Program Management International.

Cann, J. R., Blackman, D. K., Smith, D. K., McAllister, E., Janssen, B., Mello, S., et al. (1997). Corrugated slip surfaces formed at ridge–transform intersections on the mid-Atlantic ridge. *Nature*, *385*, 329–332. https://doi.org/10.1038/385329a0

Cannat, M., Mével, C., & Stakes, D. (1991). Normal ductile shear zones at an oceanic spreading ridge: Tectonic evolution of Site 735 gabbros (Southwest Indian Ocean). In R. P. Von Herzen, P. T. Robinson, et al. (Eds.), *Proceedings of the Ocean Drilling Program*, *Scientific Results* (Vol. 118, pp. 415–429). College Station, TX: Ocean Drilling Program.

Carmichael, I. S. E., & Ghiorso, M. S. (1986). Oxidation-reduction relations in basic magma: A case for homogeneous equilibria. *Earth and Planetary Science Letters*, *78*, 200–210. https://doi.org/10.1016/0012-821X(86)90061-0

Chen, Y., Niu, Y., Wang, X., Gong, H., Guo, P., Gao, Y., & Shen, F. (2019). Petrogenesis of ODP hole 735B (leg 176) oceanic plagiogranite: Partial melting of gabbros or advanced extent of fractional crystallization? *Geochemistry, Geophysics, Geosystems*, *20*, 2717–2732. https://doi.org/10.1029/2019GC008320

Christie, D. M., Carmichael, I. S. E., & Langmuir, C. H. (1986). Oxidation states of mid-ocean ridge basalt glasses. *Earth and Planetary Science Letters*, *79*, 397–411. https://doi.org/10.1016/0012-821X(86)90195-0

Coleman, R. G., & Peterman, Z. E. (1975). Oceanic plagiogranite. *Journal of Geophysical Research*, *80*(8), 1099–1108. https://doi.org/10.1029/JB080i008p01099

Coogan, L. A., Wilson, R. N., Gillis, K. M., & MacLeod, C. J. (2001). Near-solidus evolution of oceanic gabbros: Insights from amphibole geochemistry. *Geochimica et Cosmochimica Acta*, *65*(23), 4339–4357. https://doi.org/10.1016/S0016-7037(01)00714-1

Deans, J. R. L., & Yoshinobu, A. S. (2019). Geographically re-oriented magmatic and metamorphic foliations from ODP hole 735B Atlantis Bank, Southwest Indian ridge: Magmatic intrusion and crystal-plastic overprint in the footwall of an oceanic core complex. *Journal of Structural Geology*, *126*, 1–10. https://doi.org/10.1016/j.jsg.2019.05.001

deMartin, B. J., Sohn, R. A., Canales, J. P., & Humphris, S. E. (2007). Kinematics and geometry of active detachment faulting beneath the trans-Atlantic Geotraverse (TAG) hydrothermal field on the Mid-Atlantic ridge. *Geology*, *35*, 711–714. https://doi.org/10.1130/G23718A.1

Dick, H. J. B., Bryan, W. B., & Thompson, G. (1981). Low-angle faulting and steady-state emplacement of plutonic rocks at ridge-transform intersections. *Eos*, *62*, 406. https://doi.org/10.1029/EO062i017p00201

Dick, H. J. B., Kvassnes, A. J. S., Robinson, P. T., MacLeod, C. J., & Kinoshita, H. (2019). The Atlantis Bank gabbro massif, Southwest Indian ridge. *Progress in Earth and Planetary Science*, *6*, 1–70. https://doi.org/10.1186/s40645-019-0307-9

Dick, H. J. B., MacLeod, C. J., Blum, P., Abe, N., Blackman, D. K., Bowles, J. A., et al. (2019). Dynamic accretion beneath a slow-spreading ridge segment: IODP Hole 1473A and the Atlantis Bank oceanic Core complex. *Journal of Geophysical Research: Soild Earth*, *124*, 12,631–12,659. https://doi.org/10.1029/2018JB016858

Dick, H. J. B., Meyer, P. S., Bloomer, S. H., Kirby, S., Stakes, D. S., & Mawer, C. (1991). Lithostratigraphic evolution of an in-situ section of oceanic layer 3. In R. P. Von Herzen, P. T. Robinson, et al. (Eds.), *Proceedings of the Ocean Drilling Program*, *Scientific Results* (Vol. 118, pp. 439–538). College Station, TX: Ocean Drilling Program.

Dick, H. J. B., Natland, J. H., Alt, J. C., Bach, W., Bideau, D., Gee, J. S., et al. (2000). A long in situ section of the lower ocean crust: Results of ODP leg 176 drilling at the Southwest Indian ridge. *Earth and Planetary Science Letters*, *179*(1), 31–51. https://doi.org/10.1016/S0012-821X(00)00102-3

Dick, H. J. B., Natland, J. H., Miller, D. J., Alt, J. C., Bach, W., Bideau, D., et al. (1999). Site 735. In H. J. B. Dick, J. H. Natland, D. J. Miller, et al. (Eds.), *Proceedings of the Ocean Drilling Program, initial reports* (Vol. 176, pp. 1–314). College Station, TX: Ocean Drilling Program.

Dick, H.J.B., Robinson, P.T., & Meyer, P.S. (1992), The plutonic foundation of a slow-spreading ridge. In R. A. Duncan, et al. (Eds.), *Synthesis of results from scientific drilling in the Indian Ocean*: *Geophysical Monograph* (Vol. 70, pp. 1–39). Washington, DC: American Geophysical Union.

Dick, H. J. B., Schouten, H., Meyer, P. S., Gallo, D. G., Bergh, H., Tyce, R., et al. (1991). Tectonic evolution of the Atlantis II fracture zone. In R. P. Von Herzen, P. T. Robinson, et al. (Eds.), *Proceedings of the Ocean Drilling Program*, *Scientific Results* (Vol. 118, pp. 359–398). College Station, TX: Ocean Drilling Program.

Dixon, S., & Rutherford, M. J. (1979). Plagiogranites as late-stage immiscible liquids in ophiolite and mid-ocean ridge suites: An experimental study. *Earth and Planetary Science Letters*, *45*(1), 45–60. https://doi.org/10.1016/0012-821X(79)90106-7

Feig, S. T., Koepke, J., & Snow, J. E. (2006). Effect of water on tholeiitic basalt phase equilibria: An experimental study under oxidizing conditions. *Contributions to Mineralogy and Petrology*, *152*(5), 611–638. https://doi.org/10.1007/s00410-006-0123-2

Flagler, P. A., & Spray, J. G. (1991). Generation of plagiogranite by amphibolite anatexis in oceanic shear zones. *Geology*, *19*(1), 70–73. https://doi.org/10.1130/0091-7613(1991)019%3C0070:GOPBAA%3E2.3.CO;2

Gao, Y., Hoefs, J., Hellebrand, E., von der Handt, A., & Snow, J. (2007). Trace element zoning in pyroxenes from ODP Hole 735B gabbros: Diffusive exchange or synkinematic crystal fractionation? *Contributions to Mineralogy and Petrology*, *153*, 429–442. https://doi.org/10.1007/s00410-006-0158-4

Gillis, K. M., & Meyer, P. S. (2001). Metasomatism of oceanic gabbros by late stage melts and hydrothermal fluids: Evidence from the rare earth element composition of amphiboles. *Geochemistry, Geophysics, Geosystems*, *2*(3), 1012. https://doi.org/10.1029/2000GC000087

Grimes, C. B., Ushikubo, T., John, B. E., & Valley, J. W. (2011). Uniformly mantle-like $\delta^{18}O$ in zircons from oceanic plagiogranites and gabbros. *Contributions to Mineralogy and Petrology*, *161*, 13–33. https://doi.org/10.1007/s00410-010-0519-x

Holland, T., & Blundy, J. (1994). Non-ideal interactions in calcic amphiboles and their bearing on amphibole-plagioclase thermometry. *Contributions to Mineralogy and Petrology*, *116*, 433–447. https://doi.org/10.1007/BF00310910

Hosford, A., Tivey, M., Matsumoto, T., Dick, H., Schouten, H., & Kinoshita, H. (2003). Crustal magnetization and accretion at the southwest Indian ridge near the Atlantis II fracture zone, 0–25 ma. *Journal of Geophysical Research*, *108*(B3), 2169. https://doi.org/10.1029/2001JB000604

John, B. E., Foster, D. A., Murphy, J. M., Cheadle, M. J., Baines, A. G., Fanning, C. M., & Copeland, P. (2004). Determining the cooling history of in situ lower oceanic crust—Atlantis Bank, SW Indian ridge. *Earth and Planetary Science Letters*, *222*(1), 145–160. https://doi.org/10.1016/j.epsl.2004.02.014

Juster, T. C., Grove, T. L., & Perfit, M. R. (1989). Experimental constraints on the generation of FeTi basalts, andesites, and rhyodacites at the Galapagos spreading Center, 85°W and 95°W. *Journal of Geophysical Research*, *94*(B7), 9251–9274. https://doi.org/10.1029/JB094iB07p09251

Karson, J. A., & Dick, H. J. B. (1983). Tectonics of ridge-transform intersections at the Kane Fracture Zone. *Marine Geophysical Researches*, *6*, 51–98. https://doi.org/10.1007/BF00300398

Kendrick, M. A. (2019). Halogens in Atlantis Bank gabbros, SW Indian ridge: Implications for styles of seafloor alteration. *Earth and Planetary Science Letters*, *514*, 96–107. https://doi.org/10.1016/j.epsl.2019.02.034

Kikawa, E., & Pariso, J. E. (1991). Magnetic properties of gabbros from Hole 735B, Southwest Indian Ridge. In R. P. Von Herzen, P. T. Robinson, et al. (Eds.), *Proceedings of the Ocean Drilling Program*, *Scientific Results* (Vol. 118, pp. 285–307). College Station, TX: Ocean Drilling Program.

Koepke, J., Berndt, J., Feig, S. T., & Holtz, F. (2007). The formation of SiO_2-rich melts within the deep oceanic crust by hydrous partial melting of gabbros. *Contributions to Mineralogy and Petrology*, *153*(1), 67–84. https://doi.org/10.1007/s00410-006-0135-y

Koepke, J., Botcharnikov R.E., Natland J.H. (2018). Crystallization of late-stage MORB under varying water activities and redox conditions: Implications for the formation of highly evolved lavas and oxide gabbro in the ocean crust. *Lithos*, *323*, 58–77. http://doi.org/10.1016/j.lithos.2018.10.001

Koepke, J., Feig, S., & Snow, J. (2005). Late stage magmatic evolution of oceanic gabbros as a result of hydrous partial melting: Evidence from the Ocean Drilling Program (ODP) Leg 153 drilling at the Mid-Atlantic ridge. *Geochemistry, Geophysics, Geosystems*, *6*, Q02001. https://doi.org/10.1029/2004GC000805

Koepke, J., Feig, S. T., Snow, J., & Freise, M. (2004). Petrogenesis of oceanic plagiogranites by partial melting of gabbros: An experimental study. *Contributions to Mineralogy and Petrology*, *146*(4), 414–432. https://doi.org/10.1007/s00410-003-0511-9

Lissenberg, C. J., & MacLeod, C. J. (2016). A reactive porous flow control on mid-ocean ridge magmatic evolution. *Journal of Petrology*, *57*(11&12), 2195–2220. https://doi.org/10.1093/petrology/egw074

MacLeod, C. J., Dick, H. J. B., Blum, P., Abe, N., Blackman, D. K., Bowles, J. A., et al. (2017a). Site U1473. In C. J. MacLeod, H. J. B. Dick, P. Blum, the Expedition 360 Scientists, & Southwest Indian Ridge Lower Crust and Moho (Eds.), *Proceedings of the International Ocean Discovery Program* (Vol. 360, pp. 1–136). College Station, TX: International Ocean Discovery Program. https://doi.org/10.14379/iodp.proc.360.103.2017

MacLeod, C. J., Dick, H. J. B., Blum, P., Abe, N., Blackman, D. K., Bowles, J. A., et al. (2017b). Expedition 360 methods. In C. J. MacLeod, H. J. B. Dick, P. Blum, the Expedition 360 Scientists, & Southwest Indian Ridge Lower Crust and Moho (Eds.), *Proceedings of the International Ocean Discovery Program* (Vol. 360, pp. 1–51). College Station, TX: International Ocean Discovery Program. https://doi.org/10.14379/iodp.proc.360.102.2017

MacLeod, C. J., Searle, R. C., Murton, B. J., Casey, J. F., Mallows, C., Unsworth, S. C., et al. (2009). Life cycle of oceanic core complexes. *Earth and Planetary Science Letters*, *287*, 333–344. https://doi.org/10.1016/j.epsl.2009.08.016

Mathieu, L., Van Wyk De Vries, B., Holohan, E. P., & Troll, V. R. (2008). Dykes, cups, saucers and sills: Analogue experiments on magma intrusion into brittle rocks. *Earth and Planetary Science Letters*, *271*, 1–13. https://doi.org/10.1016/j.epsl.2008.02.020

Mehl, L., & Hirth, G. (2008). Plagioclase preferred orientation in layered mylonites: Evaluation of flow laws for the lower crust. *Journal of Geophysical Research*, *113*, B05202. https://doi.org/10.1029/2007JB005075

Michael, P., & Schilling, J.-G. (1989). Chlorine in mid-ocean ridge magmas: Evidence for assimilation of seawater-influenced components. *Geochimica et Cosmochimica Acta*, *53*, 3131–3143. https://doi.org/10.1016/0016-7037(89)90094-X

Miranda, E. A., & John, B. E. (2010). Strain localization along the Atlantis Bank oceanic detachment fault system, southwest Indian ridge. *Geochemistry, Geophysics, Geosystems*, *11*, Q04002. https://doi.org/10.1029/2009GC002646

Morris, A., Bowles, J. A., Tivey, M., & Expedition 360 Scientists. (2016), Paleomagnetic constraints on the evolution of Atlantis Bank: Results from IODP Expedition 360 "SW Indian Ridge Lower Crust and Moho". *AGU*, abstract #OS31D-2059.

Morris, A., Gee, J. S., Pressling, N., John, B. E., MacLeod, C. J., Grimes, C. B., & Searle, R. C. (2009). Footwall rotation in an oceanic core complex quantified using reoriented Integrated Ocean drilling program core samples. *Earth and Planetary Science Letters*, *287*, 217–228. https://doi.org/10.1016/j.epsl.2009.08.007

Mutter, J. C., & Karson, J. A. (1992). Structural processes at slow-spreading ridges. *Science*, *257*(5070), 627–634. https://doi.org/10.1126/science.257.5070.627

Natland, J. H., & Dick, H. J. B. (2001). Formation of the lower ocean crust and the crystallization of gabbroic cumulates at a very slowly spreading ridge. *Journal of Volcanology and Geothermal Research*, *110*, 191–233. https://doi.org/10.1016/S0377-0273(01)00211-6

Natland, J. H., Meyer, P. S., Dick, H. J. B., & Bloomer, S. H. (1991). Magmatic oxides and sulfides in gabbroic rocks from Hole 735B and the later development of the liquid line of descent. In R. P. Von Herzen, P. T. Robinson, et al. (Eds.), *Proceedings of the Ocean Drilling Program*, *Scientific Results* (Vol. 118, pp. 75–111). College Station, TX: Ocean Drilling Program.

Nguyen, D. K., Morishita, T., Soda, Y., Tamura, A., Ghosh, B., Harigane, Y., et al. (2018). Occurrence of felsic rocks in oceanic gabbros from IODP Hole U1473A: Implications for evolved melt migration in the lower oceanic crust. *Minerals*, *8*, 583. https://doi.org/10.3390/min8120583

Niu, Y., Gilmore, T., Mackie, S., Greig, A., & Bach, W. (2002). Mineral chemistry, whole-rock compositions, and petrogenesis of Leg 176 gabbros: Data and discussion. In J. H. Natland, H. J. B. Dick, D. J. Miller, & R. P. Von Herzen (Eds.), *Proceedings of the Ocean Drilling Program*, *Scientific Results* (Vol. 176, pp. 1–60). College Station, Texas: Ocean Drilling Program.

Parnell-Turner, R., Sohn, R. A., Peirce, C., Reston, T. J., MacLeod, C. J., Searle, R. C., & Simão, N. M. (2017). Oceanic detachment faults generate compression in extension. *Geology*, *45*(10), 923–926. https://doi.org/10.1130/G39232.1

Passchier, C. W., & Trouw, R. A. J. (2005). *Microtectonics*. New York: Springer Verlag.

Pietranik, A., Storey, C., Koepke, J., & Lasalle, S. (2017). Zircon record of fractionation, hydrous partial melting and thermal gradients at different depths in oceanic crust (ODP Site 735B, South-West Indian Ocean). *Contributions to Mineralogy and Petrology*, *172*(10), 1–16. https://doi.org/10.1007/s00410-016-1324-y

Pollard, D. D. (1973). Derivation and evaluation of a mechanical model for sheet intrusions. *Tectonophysics*, *19*(3), 233–269. https://doi.org/10.1016/0040-1951(73)90021-8

Rioux, M., Cheadle, M. J., John, B. E., & Bowring, S. A. (2016). The temporal and spatial distribution of magmatism during lower crustal accretion at an ultraslow-spreading ridge: High-precision U-Pb zircon dating of ODP Holes 735B and 1105A, Atlantis Bank, southwest Indian ridge. *Earth and Planetary Science Letters*, *449*, 395–406. https://doi.org/10.1016/j.epsl.2016.05.047

Robinson, P. T., Von Herzen, R., Adamson, A. C., Becker, K., Bloomer, S. H., Cannat, C., et al. (1989). *Proceedings of the Ocean Drilling Program, initial reports* (Vol. 118). College Station, TX: Ocean Drilling Program.

Sanfilippo, A., Tribuzio, R., Antonicelli, M., & Zanetti, A. (2017), Amphibole and felsic veins from the gabbroic oceanic core complex of Atlantis Bank (Southwest Indian Ridge, IODP Hole U1473A): When the fluids meets the melts. *American Geophysical Union*, abstract #V43D-0556.

Schultz-Ela, D. D., Jackson, M. P. A., & Vendeville, B. C. (1993). Mechanics of active salt diapirism. *Tectonophysics*, *228*, 275–312. https://doi.org/10.1016/0040-1951(93)90345-K

Schwartz, J. J., John, B. E., Cheadle, M. J., Miranda, E. A., Grimes, C. B., Wooden, J. L., & Dick, H. J. B. (2005). Dating the growth of oceanic crust at a slow-spreading ridge. *Science*, *310*(5748), 654–657. https://doi.org/10.1126/science.1116349

Toplis, M. J., & Carroll, M. R. (1995). An experimental study of the influence of oxygen fugacity on Fe-Ti oxide stability, phase relations, and mineral-melt equilibria in ferro-basaltic systems. *Journal of Petrology*, *36*(5), 1137–1170. https://doi.org/10.1093/petrology/36.5.1137

Tribuzio, R., Tiepolo, M., & Thirlwall, M. F. (2000). Origin of titanian pargasite in gabbroic rocks from the Northern Apennine ophiolites (Italy): Insights into the late-magmatic evolution of a MOR-type intrusive sequence. *Earth and Planetary Science Letters*, *176*, 281–293. https://doi.org/10.1016/S0012-821X(00)00014-5

Vanko, D. A., & Stakes, D. S. (1991). Fluids in oceanic layer 3: Evidence from veined rocks, Hole 735B, Southwest Indian Ridge. In R. P. Von Herzen, P. T. Robinson, et al. (Eds.), *Proceedings of the Ocean Drilling Program*, *Scientific Results* (Vol. 118, pp. 181–215). College Station, TX: Ocean Drilling Program.

Wilson, D. S., Teagle, D. A. H., Alt, J. C., Banerjee, N. R., Umino, S., Miyashita, S., et al. (2006). Drilling to gabbro in intact ocean crust. *Science*, *312*(5776), 1016–1020. https://doi.org/10.1126/science.1126090

Yoshinobu, A. S., & Hirth, G. (2002). Microstructural and experimental constraints on the rheology of partially molten gabbro beneath oceanic spreading centers. *Journal of Structural Geology*, *24*(6–7), 1101–1107. https://doi.org/10.1016/S0191-8141(01)00094-3

Zhou, Y., Rybacki, E., Wirth, R., He, C., & Dresen, G. (2012). Creep of partially molten fine-grained gabbro under dry conditions. *Journal of Geophysical Research*, *117*, B05204. https://doi.org/10.1029/2011JB008646

Zimmer, M. M., Plank, T., Hauri, E. H., Yogodzinski, G. M., Stelling, P., Larsen, J., et al. (2010). The role of water in generating the calc-alkaline trend: New volatile data for Aleutian magmas and a new tholeiitic index. *Journal of Petrology*, *51*(12), 2411–2444. https://doi.org/10.1093/petrology/egq062